DISSOLVED GASES AND ISOTOPES AS TOOLS FOR AQUIFER CHARACTERIZATION IN MARTIS VALLEY

A University Thesis Presented to the Faculty

of

California State University, East Bay

In Partial Fulfillment

of the Requirements for the Degree

Master of Science in Geology

By

Daniel Concannon Segal

June, 2013

ABSTRACT

The Martis Valley groundwater basin, near Lake Tahoe, is experiencing increasing water demand and likely changes in the amount and timing of snowmelt due to global warming. Groundwater is the exclusive water supply for drinking water in the town of Truckee and surrounding ski resorts and for golf course irrigation. The objective of this study is to provide insight into the age, source, and recharge conditions of the Martis Valley groundwater basin by sampling production wells for: 1) tritium and helium isotopes to determine groundwater sources and age, 2) dissolved noble gases to determine recharge temperatures and the amount of excess air and 3) stable isotopes to determine groundwater source. Sampling events took place during winter 2011-2012, June 2012, and September 2012 to assess seasonal variation in groundwater and potential vulnerability to climate change.

Noble gas concentrations and the ratio $^{3}He/^{4}He$ were measured using cryogenic separation and static mass spectrometry at Lawrence Livermore National Laboratory. Tritium contents were determined by degassing and tritiogenic ^{3}He accumulation, measured by static mass spectrometry.

Water temperature was found to increase between snowmelt runoff and groundwater recharge as well as between groundwater recharge and discharge. Recharge temperatures were found to be similar to mean annual air temperatures at lower elevations of Martis Valley, suggesting that most recharge is occurring at lower elevations after equilibrating in the vadose zone. Mean integrated groundwater flow depth for each well was estimated by calculating the depth the water would need to reach

in order to increase its recharge temperature to its discharge temperature using a standard geothermal gradient. Low levels of excess air found in groundwater suggest the bulk of recharge is occurring in the valley floor alluvium rather than through fractures in the mountain block. Many wells contained large amounts of excess helium from terrigenic sources, including mantle helium and radiogenic helium. The Polaris Fault was identified as a possible source of mantle helium. Mantle helium originating from the Polaris Fault can be used to trace groundwater flow directions and mixing of different groundwater sources. Terrigenic helium and tritium concentrations were used to determine the amount of mixing between the younger and older groundwater sources that were found in these long screened production wells. Recharge temperatures, amount of excess air, and tritium concentrations were found to vary between sampling events, especially in wells with younger groundwater (as indicated by higher tritium concentrations) and shallower flow depths (as indicated by small differences between recharge and discharge temperatures). These seasonal variations suggest that changes in the timing and amount of recharge under future warmer climate conditions will rather quickly impact at least a portion of the aquifer system in Martis Valley.

ACKNOWLEDGMENTS

I would like to acknowledge Dr. Jean Moran, Dr. Ate Visser, Dr. Bradley Esser, and Dr. Michael Singleton for their valuable input and mentoring.

DISSOLVED GASES AND ISOTOPES AS TOOLS FOR

AQUIFER CHARACTERIZATION IN MARTIS VALLEY

By

Daniel Concannon Segal

Approved:	Date:
Dr. Jean Moran	5/30/13
Dr. Luther Strayer	5/28/2013
Dr. Ate Visser	5/22/2013

TABLE OF CONTENTS

LIST OF FIGURES

LIST OF TABLES

INTRODUCTION

California relies heavily on groundwater to support its growing population and thriving agriculture industry. Seasonal snowmelt contributes significantly to recharge in alpine and subalpine groundwater basins, and makes up a significant portion of the runoff in the major rivers draining the Sierra Nevada. Predicted increasing temperatures from climate change will cause a greater proportion of precipitation in California to occur as rain, decrease the amount of snowpack in the Sierra Nevada, and shift the snowmelt hydrograph to an earlier and sharper peak (Earman and Dettinger, 2007). This will increase the likelihood of flooding events and likely cause a decrease in groundwater recharge of snowmelt, since more snowmelt will leave the watershed as surface water. Climate change presents challenges to managing the water supply, since it will have an effect on how much groundwater is recharging, where it's recharging, and by what mechanism recharge is occurring. By understanding current seasonal groundwater recharge conditions and residence times in high elevation basins where climate change is likely to affect precipitation and runoff, we can assess its vulnerability to climate change (Earman and Dettinger, 2007; Singleton and Moran, 2010) .

Martis Valley has been identified as a region likely to face water shortages in the future and has been selected to study how climate change is impacting California's groundwater supply. Martis Valley is a high elevation basin in the Sierra Nevada which depends entirely on groundwater to provide drinking water to the town of Truckee and the surrounding region. Martis Valley's economy is sustained by tourism and groundwater is the exclusive source for providing irrigation for golf courses in summer

and for creating artificial snow at ski resorts in winter. Despite heavy reliance and development of groundwater resources, relatively little is known about the groundwater system. Climate change presents a unique challenge for managing the municipal groundwater supplies in Martis Valley. Understanding seasonal variability of the aquifer can be useful in predicting the potential impact climate change will have on Martis Valley's groundwater supply. Dissolved gas and isotope analysis have the potential to add new and unique information about Martis Valley's groundwater systems to assess the regional groundwater supply's vulnerability to climate change.

Noble gas concentrations are used to examine recharge conditions, including recharge temperatures and excess air concentrations. Tritium and helium-3 measurements can be used in determining the average age of a groundwater sample that is less than 50 years old, when circumstances allow for quantification of the various helium components. Stable isotopes of oxygen and hydrogen in water molecules are useful in determining the sources of groundwater recharge.

BACKGROUND

Geologic Setting

Martis Valley is a structural basin north of Lake Tahoe in the Walker Lane Belt shear zone, a transitional zone between the Sierra Nevada Mountains and the Basin and Range Geomorphic Provinces (Brown&Caldwell, 2013). The lowest terrace in the valley floor is at 5,700 feet (1737 m) elevation. Mountains rise dramatically to the south including the 8,742 feet (2665 m) elevation Martis Peak. The Martis Valley groundwater basin lies between the Sierra Nevada crest in the west and the Carson Range to the east. Extensional Basin and Range-style normal faulting, as well as Walker Lane Belt associated strike-slip faulting formed this structural valley during the Pliocene and early Pleistocene as the Sierra Nevada uplifted about 5,000 feet (1524 m) relative to the graben. Most structural development has occurred during the last five million years and active faulting continues to this day. The bedrock of the Tahoe Basin area consists of primarily Mesozoic Sierra Nevada Batholith granodiorite that was uplifted by the Sierra Nevada and Carson Ranges. Volcanic activity occurred in Martis Valley leaving thick sequences of late Miocene to Pleistocene aged volcanic rock. These sequences overlie the bedrock in the Martis Valley watershed area and include older andesite tuffs, breccias, and flows, as well as younger cinder cones, basalts and latite flows. Four major glacial events shaped the topography of Martis Valley during the Pleistocene. Glacial moraines and outwash plain sediments from the Tahoe and Tioga glaciations fill much of the Martis Valley basin (Fram et al., 2009). A stratigraphic section for Martis Valley is shown in Figure 1.

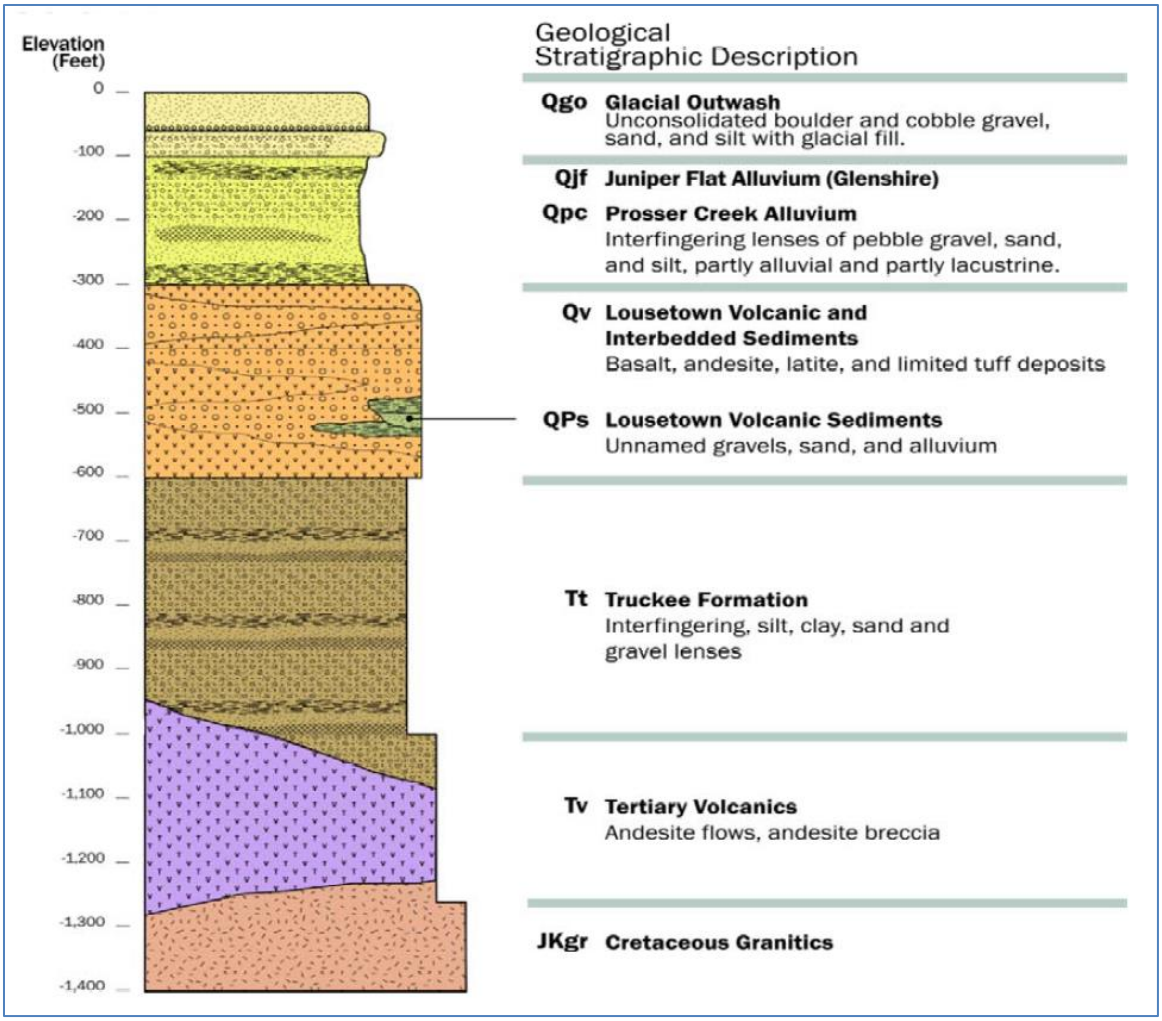

Figure 1: Martis Valley stratigraphy consists of granitics overlaid by volcanic sediments, alluvium, and glacial deposits. This complicated stratigraphy allows for multiple aquifer units with varying connectivity (Brown&Caldwell, 2013).

Hydrogeologic Conditions

The Martis Valley watershed occupies an area of 57 square miles (147.6 square km) in Nevada and Placer counties. Groundwater is managed by the Placer County Water Agency (PCWA) and the Truckee Donner Public Utility District (TDPUD). The local

water agencies include the public PCWA as well as private TDPUD, Glenshire MWC, Donner Lake WC, and Northstar CSD (California Groundwater Bulletin 118, 2006). The Truckee River flows SW to NE across Martis Valley and is controlled by a dam at the edge of Lake Tahoe. Flows in the Truckee River are managed by the Truckee River Operating agreement (Coulter et al., 2009).

The groundwater bearing units in Martis Valley are up to 1,200 feet (366 m) thick and are comprised of interlayered Miocene to late Pleistocene volcanic and sedimentary deposits. Low-permeability Miocene volcanic rocks form the base of the water bearing units. Basin-fill volcanic units include andesite lava, tuff, and breccia. Sediments originating from the volcanic and volcaniclastic units surrounding Martis Valley comprise the glacial, lacustrine, and fluvial sedimentary deposits. These sedimentary deposits provide the most groundwater storage and best opportunity for extraction. These units also include relatively impermeable laterally extensive clay and silt layers (California Groundwater Bulletin 118, 2006). Roughly half of the surface of Martis Valley is covered in glacial outwash sediments that are up to 150 feet (46 m) thick. The basin's stratigraphy is divided into lower and upper aquifer systems. The lower aquifer system is found in the Truckee formation while the upper aquifer system consists of the shallower glacial and alluvium deposits. These units are thought to have limited interconnectivity with the Lousetown volcanic units acting as a barrier to flow (Figure 1). The source most of the groundwater recharge begins as rain and snow melt in Martis Valley and the surrounding mountains (Fram et al., 2009). Wells have been found to be artesian in southern Martis Valley, indicating confined conditions over some portion of

the aquifer system. These wells are also situated near faults, which are interpreted as barriers to groundwater flow (Brown&Caldwell, 2013). Thermal springs are found in this region, adjacent to the recently-mapped Polaris Fault (Hunter et al., 2011).

Annual groundwater levels have remained relatively constant from 1990 through 2000 with seasonal water level variations often exceeding 10 feet (3 m). Longer term water level variations can additionally exceed 10 feet (3 m). The water level elevation is controlled by the hydrogeologic units' complex stratigraphy, topography, and groundwater flow barriers. The Martis Valley basin's current groundwater storage has been estimated at 484,000 acre-feet (5.97×10^8 m^3). The total basin volume was estimated at 9,680,000 acre-feet (1.19×10^{10} m^3) with an average unconfined storativity of 0.05. Annual groundwater recharge is estimated at 23,829 acre-feet (2.9×10^7 m^3) from precipitation and 5,433 acre-feet (2.9×10^6 m^3) from artificial recharge at a wastewater treatment facility east of Truckee. Urban extraction of groundwater is estimated at 7,062 acre-feet (8.71×10^6 m^3) per year. 1,274 acre-feet (1.57×10^6 m^3) of the extracted groundwater is used to irrigate golf courses, which very little, if any, of which will contribute to groundwater recharge. Subsurface inflow and outflow are estimated at 5,336 acre-feet (6.6×10^6 m^3) and 17,639 acre-feet (2.2×10^7 m^3) per year (Nimbus Engineers, 2001). More recent groundwater recharge estimates of 32,745-35,168 acre-feet (4.0×10^7-4.3×10^7 m^3) per year have been generated by Desert Research Institute's Martis Valley integrated groundwater, surface water, and climate change model (Huntington et al., 2013). While current annual groundwater extraction is only about 30% of groundwater recharge, future scenarios predict higher demand and potentially lower recharge.

Climate

The climate in Martis Valley consists of warm dry summers and cold, wet, and snowy winters. Average precipitation is 30-35 inches (76-89 cm) per year (Fram et al., 2009). Most precipitation occurs as snow between April and October. Streamflow peaks in May or June during spring snowmelt. Summer thunderstorms account for a small proportion of annual precipitation. Temperature ranges from average lows of 15°F (-9°C) in December to average highs of 82°F (28°C) in July. Martis Valley's climate is highly variable on a decadal timescale with longer dry periods (e.g., 1971-1978, 1987-1994) and shorter, more extreme wet periods (e.g., 1962-1965, 1982-1983). Climate change projections by the National Oceanic and Atmospheric Association predict a shift from snowfall to rain at the valley floor elevation due to increasing global temperatures. This potentially increases the frequency and magnitude of flooding, causing more water to leave the basin rather than infiltrating and recharging groundwater (Brown&Caldwell, 2013).

FIELD AND LABORATORY PROCEDURES

Tritium and dissolved noble and abundant gas samples were collected from production wells located in Martis Valley operated by Truckee-Donner Public Utility District, Northstar Community Services District, and the Placer County Water Agency. Most production wells were currently operating so no purging was necessary. Pumping rates ranged between 1136 L/min (300 gal/min) to 5678 L/min (1500 gal/min). Well water was collected from a spigot at the well head at about 3.79 liter (1 gal) per minute

and water was directed into a YSI 556 flow-through cell equipped with sensors measuring water quality parameters. These parameters include temperature, conductivity, pH, dissolved oxygen, oxidation-reduction potential, and turbidity. After the parameters stabilized these measurements as well as the time were recorded and sampling began.

Dissolved noble gas concentrations are collected in $^{3}/_{8}$ inch (0.95 cm) diameter copper tubes that hold approximately 9.75 mL of groundwater. Each copper tube is held in place with two clamps affixed to an aluminum back plate. A vinyl tube connects the well sample port to the copper tube, fastening together with hose clamps. A second vinyl tube connects the water exiting the cooper tube to a valve. While water is flowing through, the copper tube is tapped to free any bubbles that may be trapped inside the copper tube. The valve is then partially shut to create back pressure in the copper tube. The clamps are then tightened to pitch to copper tube shut at each end, collecting inside a groundwater sample under pressure and free of any contamination from atmospheric gases (Figure 2). Abundant gas samples are collected in 40 mL Volatile Organic Analysis (VOA) vials. VOA vials are filled under laminar flow conditions and are closed leaving no headspace. The VOAs need to be immediately put on ice for transport back to the lab. Tritium samples are collected by filling a 1 liter Pyrex container. Stable isotopes of oxygen and hydrogen are sampled in 50 mL glass containers. Two copper tubes, two voas, and one 1L sample are collected from each well. No chemical preservatives need to be added to any of these samples.

Figure 2: Dissolved noble gas samples are collected by pumping groundwater through 9.5mm (3/8 in) copper tubes and then clamping the copper tubes to form a water-tight seal.

Samples are stored and measured at Lawrence Livermore National Laboratory (LLNL). VOA vials are stored in a 4 degree Celsius (39 degrees Fahrenheit) refrigerator and should be analyzed within three days for best results. Copper tubes and tritium bottles can be stored for years.

The dissolved abundant gases, including methane, nitrogen, oxygen, argon, and carbon dioxide, are measured in the VOA samples using a membrane inlet mass spectrometer (MIMs) (Singleton and Hudson, 2005). Samples are prepared by warming

the VOAs in a room temperature water bath, along with air equilibrated water standards, for 30 minutes. The MIMs systems consists of a peristaltic or syringe pump than pumps the water from the sample through a permeable membrane tube. The membrane tube runs through a vacuum causing the dissolved gases from the sample to permeate the membrane. The gases then pass through a water trap, a steel tube surrounded by a mixture of crushed dry ice and isopropanol, which works to freeze excess water vapor. The remaining gas then enters a residual gas analyzer (RGA) quadrupole mass spectrometer. Samples are measured for 5 minutes and average concentrations during the last 2 minutes of analysis are recorded. Two VOAs are measured for each well and results are averaged for the final concentration.

VOAs can also be used as sample containers for dissolved argon, krypton, and xenon, which are analyzed on the noble gas membrane inlet mass spectrometer (NGMIMs)(Visser, 2011). This system is the same as the MIMS with a few enhancements that allow greater sensitivity. Between the water trap and the mass spectrometer there is a CO_2 trap which uses a tube of zeolites to remove CO_2 from the samples as well as titanium-zircon getters which sequester most of the more abundant gases. The residual gas analyzer mass spectrometer also contains an electron multiplier to increase the sensitivity.

The noble gases helium, neon, argon, krypton, xenon, as well as the $^{3}He/^{4}He$ isotope ratio, are measured using the noble gas mass spectrometer (NGMS) (Figure 3). Samples are prepared by removing the copper tubes from their back plates and drying the tube ends with compressed nitrogen. A nut and ferrule are added to one end of the copper

tube. The tube is weighed and then tightened onto a stainless steel vessel. Nine tubes and vessels are then fastened to pneumatic valves hanging on a manifold. A bucket is placed around each of the vessels and packed half way full with dry ice. The pneumatic valves are controlled by a computer running LabVIEW software. Additional valves are used to apply vacuum to the manifold. A leak check routine is run on LabVIEW that opens and closes the valve to each vessel in sequence and checks the pressure to ensure there are no vacuum leaks. The dry ice buckets are removed. The clamp on the copper tube closest to the vessel is then removed and the pinched tube is opened, allowing the water to enter the vessel. Heat guns are positioned under each vessel for 15 minutes to release the water and dissolved gases to a gas phase. Buckets are placed around the vessels and immediately packed full of dry ice. This freezes the water leaving the formerly dissolved gases separated. The samples are then ready for automated analysis by the NGMS controlled by LabView.

The gas from one sample is introduced into the manifold by opening one of the valves. The gases first enter titanium-zircon getters to remove abundant gases, leaving only the nonreactive noble gases. The noble gases then enter a coldfinger containing activated charcoal. Liquid nitrogen is then poured onto the coldfinger until the temperature drops below 83° Kelvin and the heavy noble gases (Ar, Kr, Xe) sorb to the charcoal. Helium and neon are measured on the quadrupole mass spectrometer. Helium and neon are then frozen onto a second charcoal coldfinger cooled by liquid helium to 8° Kelvin. The helium is then released and enters the sector field mass spectrometer. The sector field mass spectrometer measures the ^{4}He isotope on a Faraday cup collector and

the ^{3}He isotope on an electron multiplier collector since ^{4}He is more abundant by several orders of magnitude. In the meanwhile, the Ar, Kr and Xe are released from the charcoal coldfinger and transferred to a bare steel coldfinger cooled by liquid nitrogen to 83° Kelvin. The argon is measured as pressure on a high sensitivity capacitance manometer (Baratron) and pumped out afterwards. The krypton and xenon are released and measured by the quadrupole mass spectrometer. Aliquots of gas from a cylinder containing an air standard are measured every few cycles to record instrument consistency.

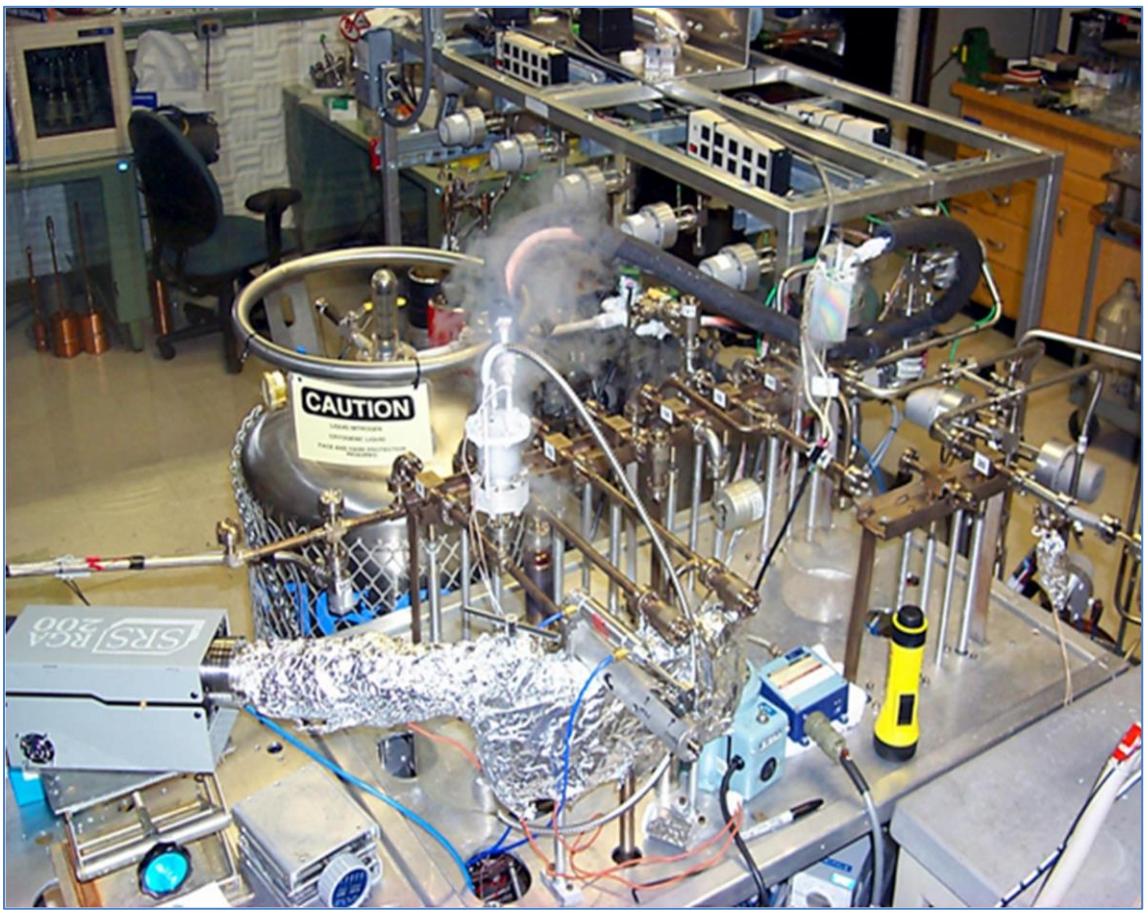

Figure 3: Lawrence Livermore National Laboratory's Noble Gas Mass Spectrometer.

Tritium is measured by the ingrowth of helium-3. 500 ml of water is poured into a stainless steel vessel. The vessels are sparged with nitrogen to remove most of the dissolved gases. Closed valves are then tightened onto the vessels and are together fastened to a manifold. Ten sample vessels hang on a manifold including one NIST standard containing a known tritium concentration. Heat guns are placed under each vessel for 15 minutes. Then ice is packed around the vessels for 1 hour. This separates out any remained dissolved gases from the water. The manifold is then placed under vacuum. Each valve is then opened in sequence allowing the gases to escape, leaving only water molecules. This heat, chill, and pump sequence is repeated a total of three times. The time of the final chill is noted as the time when no dissolved gases remain. The closed vessels are then removed from the manifold and stored for at least 3 weeks. During this time some of the tritium, which exists as part of the water molecules, decays to helium-3. The vessels are then fastened to the NGMS manifold and the newly accumulated helium-3 is measured. Using the 12.43 year half-life of tritium, the time of accumulation, and the measured helium-3 concentration, we can calculate the initial concentration of tritium in the sample at ~1 pCi/L precision (Beyerle and Du, 2000).

Stable Isotopes of Oxygen and Hydrogen are measured using an LGR Liquid Water Stable Isotope Analyzer at CSU East Bay. The LGR Liquid Water Stable Isotope Analyzer uses a cavity ringdown spectroscopy laser absorption technique to produce ratios of HOD/H_2O and H_2O^{18}/H_2O. These two ratios are used to calculate the δ^2H and $\delta^{18}O$ values for a sample, with an uncertainty of 1.0‰ and 0.3‰, respectively.

ANALYSIS

Noble gas concentrations are used to determine the recharge temperature and amount of excess air present in a sample. The equilibrium solubility of any gas, including the noble gases, is a function of temperature and pressure, defined by Henry's Law:

$$C_{eq} = \frac{p}{H(T,S)} \qquad (1)$$

where C_{eq} is the equilibrium solubility of the gas, p is the partial pressure of the gas, and H is Henry's Law constant, which is a function of temperature T and salinity S. The equilibrium solubilities of each of the noble gases under given temperatures and pressures define solubility curves for each gas (Figure 4). The proportions of noble gas concentrations measured in a sample should align with these solubility curves at the temperature at which the groundwater recharged (Mazor, 1972). Recharge temperature calculations rely heavily on xenon concentrations since xenon solubility has the strongest temperature dependence of the noble gases. Recharge temperature is useful in determining recharge location since water recharged at higher elevations, equilibrated at ambient air temperatures, should produce lower recharge temperatures, given the typical atmospheric lapse rate of 6.5°C/km (5.4°F/1000 ft).

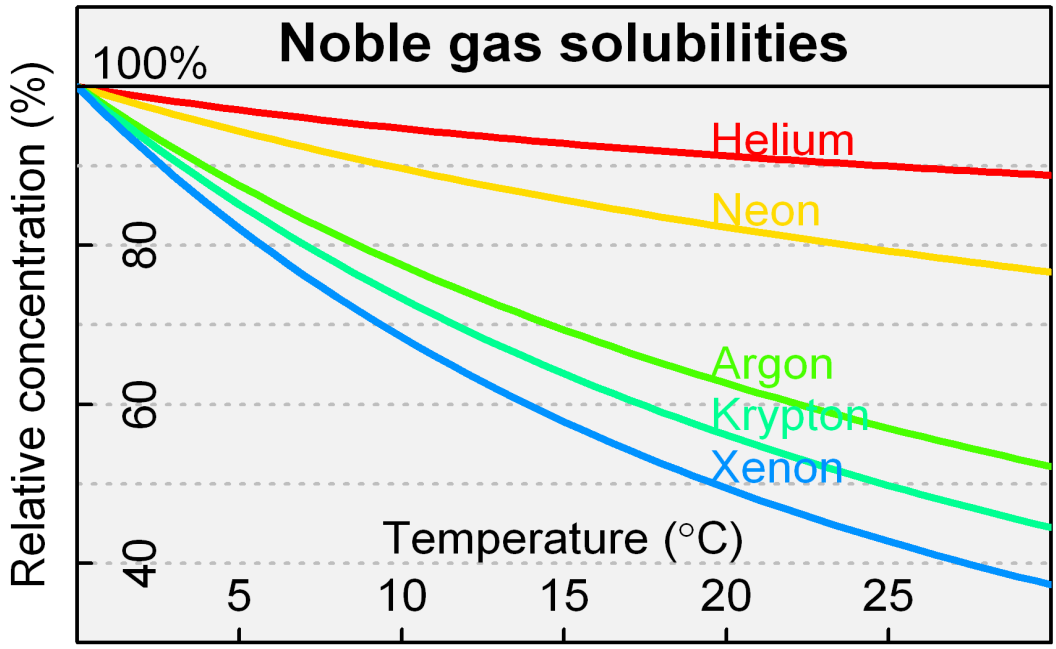

Figure 4: Curves show the relative temperature dependence of noble gas solubilities. Noble gas recharge temperatures are calculated based on this equilibrium solubility component (Benson, 1973).

However, dissolved gas concentrations in natural groundwater samples are typically in excess of what would be found for equilibrium saturation alone (Klump et al., 2007; Peeters et al., 2000). This 'excess air' is useful in examining recharge conditions. Higher levels of excess air are typically found in the mountain block, where recharge is often occurring rapidly and turbulently in fractured rock (Ajami et al., 2011; Manning and Caine, 2007). During the recharge process, quickly rising water tables cause entrained air bubbles to dissolve under increased hydrostatic pressure. In alluvial deposits, recharge may occur more slowly, under conditions of lower hydraulic head,

producing lower levels of excess air. Excess air is often expressed as ΔNe, which is the measured concentration of Ne divided by the equilibrium solubility of Ne. Neon is used to express excess air since it is the most soluble of the noble gases after helium, and unlike helium, neon is assumed to not have any terrigenic sources.

Recharge temperature and excess air are calculated together by fitting noble gas concentrations to three excess air models that have been proposed in the literature (Cey et al., 2009). These three models include partial re-equilibration (Stute et al., 1995), closed equilibrium (Aeschbach-Hertig et al., 2008), and unfractionated (Heaton and Vogel, 1981) excess air models. The unfractionated excess air model assumes that air bubbles entrapped during recharge completely dissolve, leaving the excess air component of dissolved gas with the same composition as atmospheric air. The total concentration of a dissolved gas found using the unfractionated air model (UA) is:

$$C_{Total}^{UA} = C_{eq} + A_d \cdot z \qquad (2)$$

where A_d is the concentration of dry air dissolved, and z is the volume fraction of gas in dry air. Elemental fractionation often occurs in the excess air component of dissolved gas with lighter gases being depleted relative to heavier gases. The partial re-equilibration (PR) model and closed equilibrium (CE) model attempt to explain the fractionation. The PR model suggests that complete bubble dissolution followed by diffusive degassing causes the fractionation. The total concentration of a dissolved gas found using the PR model is:

$$C_{Total}^{PR} = C_{eq} + (A_d \cdot z) \cdot e^{\frac{-R \cdot D}{D_{Ne}}} \qquad (3)$$

where A_d is initial concentration of dissolved excess air, R is degree of re-equilibration,

D is molecular diffusivity of the gas, and D_{Ne} is molecular diffusivity of Ne. The CE model suggests that incomplete dissolution of entrapped air bubbles causes the fractionation and the degree of fractionation is related to the differing gas solubilities. The total concentration of a dissolved gas found using the CE model is:

$$C_{total}^{CE} = C_{eq} + \frac{(1-F)\cdot A_e \cdot z}{1+\left(\frac{F\cdot A_e \cdot z}{C_{eq}}\right)} \qquad (4)$$

where F is the fractionation parameter and A_e is the initial concentration of entrapped air given by the following equations:

$$A_e = \frac{V_g^0}{\rho(T,S)\cdot V_w}\cdot\frac{(P_g - e_s)}{P_0} \qquad (5)$$

where V_g^0 is the initial volume of entrapped air, ρ is water density (function of temperature T and salinity S), V_w is water volume, P_g is pressure of entrapped air, e_s is the saturation water vapor pressure, and P_0 is standard pressure (1 atm). The fractionation factor, F, is given by:

$$F = \frac{v}{q} = \frac{\left(\frac{V_g}{V_g^0}\right)}{\left(\frac{P_g - e_s}{P_{atm} - e_s}\right)} \qquad (6)$$

where P_{atm} is atmospheric pressure, v is the remaining fraction of entrapped air, and q is the ratio of dry entrapped air pressure to dry atmospheric pressure (Cey et al., 2009).

Salinity is assumed to be zero for fresh groundwater and pressure is calculated using the atmospheric pressure found at the elevation of the well head. Some error will inevitably be introduced due to these assumptions, especially since the groundwater recharge elevation can differ from the well head elevation. For example, groundwater

found in a well in Martis Valley at 1800 m elevation could have potentially, but unlikely, recharged on Martis Peak at 2600 m. Due to atmospheric pressure's effect on noble gas solubilities, the noble gas recharge temperature calculated using the pressure found on Martis Peak would be 2.8°C cooler than the noble gas recharge temperature calculated using the pressure found at the well head elevation on the valley floor.

Optimal recharge temperature and excess air values are found by minimizing the values of χ^2, which represents the goodness-of-fit between measured noble gas concentrations and predicted noble gas concentrations for each excess air model. Calculations were performed using Solver, a linear programming add-in for Microsoft Excel. The model that received the highest χ^2 probability for a given sample was used to calculate that sample's recharge temperature, excess air concentration, and other derived parameters.

Only concentrations of Ne, Ar, Kr, and Xe are used in the excess air models, since they do not have significant terrigenic components. Helium in groundwater can contain terrigenic components, which can include radiogenic and mantle sources of ^3He and ^4He. Helium also may contain some tritiogenic ^3He from the decay of ^3H. The following equations show the different sources making up the total ^3He and ^4He in a groundwater sample:

$$^3He_{total} = {}^3He_{eq} + {}^3He_{ea} + {}^3He_{rad} + {}^3He_{mant} + {}^3He_{trit} \quad (7)$$

$$^4He_{total} = {}^4He_{eq} + {}^4He_{ea} + {}^4He_{rad} + {}^4He_{mant} \quad (8)$$

where He_{total} is the measured helium, He_{eq} is helium in solubility equilibrium with the atmosphere, He_{rad} is radiogenic helium produced by the alpha decay of Uranium and Thorium in the earth's crust, He_{mant} is helium produced from mantle outgassing, and $^{3}He_{trit}$ is the tritiogenic helium-3. The different components of dissolved noble gases in a typical groundwater sample are shown in Figure 5.

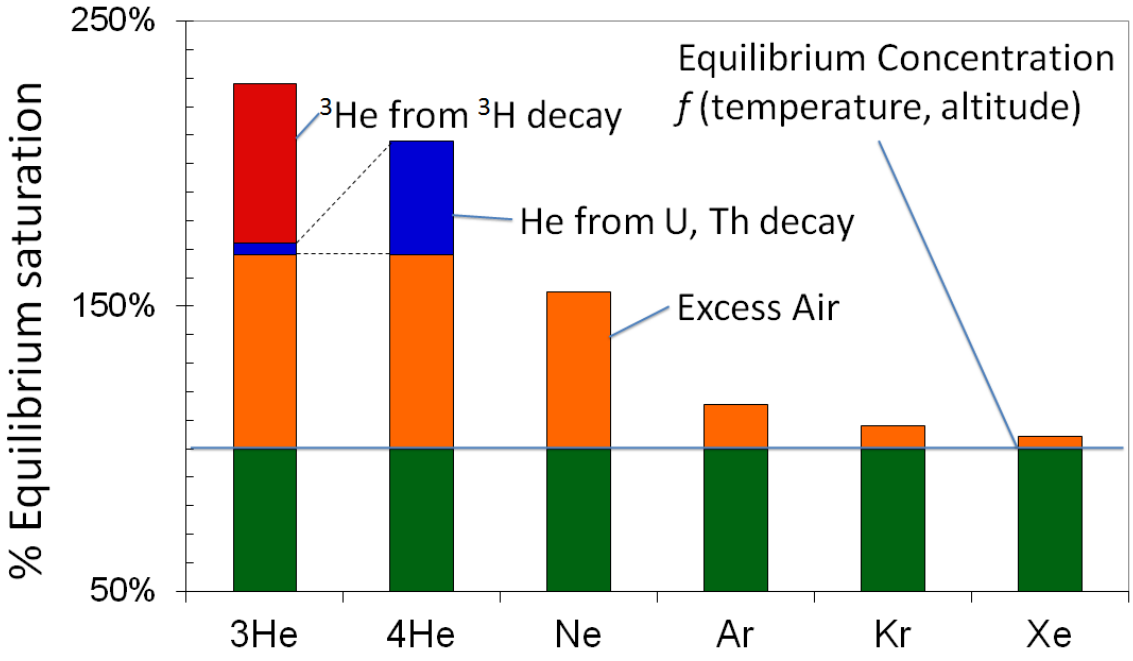

Figure 5: Sources of dissolved noble gases in a typical groundwater sample (Hudson and Moran, 2002).

Tritium and its daughter product, helium-3 are used to calculate groundwater ages of less than 50 years. Tritium is naturally produced at low levels in the atmosphere by

cosmic radiation. During the 1950s-1960s nuclear testing released much more tritium into the atmosphere. Tritium becomes part of water molecules, precipitates from clouds and then infiltrates into the ground. Tritium in the saturated zone, no longer exchanging with atmospheric tritium, decays via beta emission to ^{3}He and the He remains dissolved under closed system conditions. Tritium levels in precipitation have been decreasing since cessation of above ground nuclear weapons testing. Figure 6 shows the historical concentrations of tritium in precipitation. Apparent groundwater age can be calculated by measuring tritium and tritiogenic ^{3}He concentrations and using the following age dating equation:

$$t = \frac{T_{1/2}}{ln2} \cdot ln\left(1 + \frac{^{3}He_{trit}}{^{3}H}\right) \qquad (9)$$

where $T_{½}$ is the half-life decay of tritium, 12.43 years, $^{3}He_{trit}$ is the tritiogenic ^{3}He concentration, and ^{3}H is the concentration of tritium.

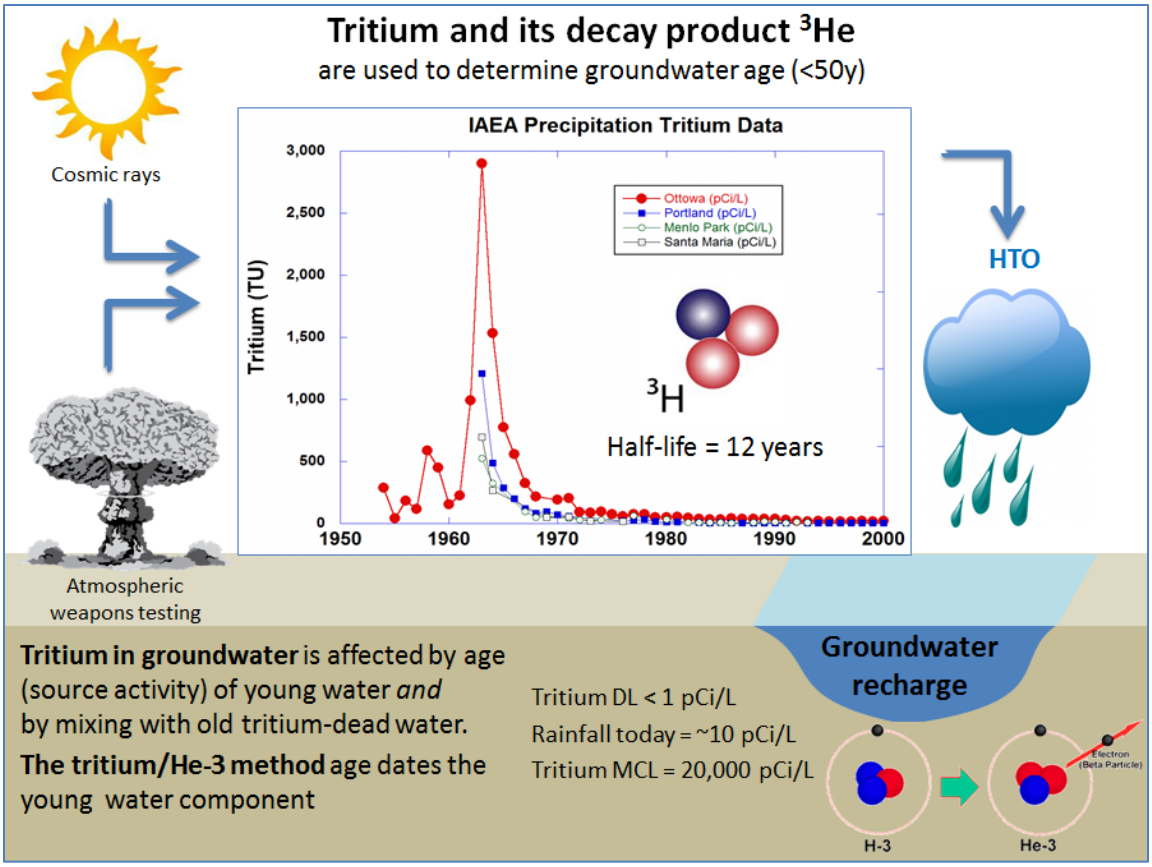

Figure 6: Cartoon showing formation of ^{3}H from cosmogenic and anthropogenic sources and its incorporation into precipitation and groundwater. Tritium and its decay product ^{3}He can be used to determine the age that precipitation (<50 years) infiltrated into the groundwater; inset graph shows historical tritium in precipitation (www-naweb.iaea.org/napc/ih/index.html).

Some ambiguities exist in calculating groundwater recharge temperatures, excess air, and especially apparent groundwater age. Groundwater samples invariably represent a mixture of several different aquifer sources with an age distribution that may span decades to thousands of years. This is especially true when sampling long screened wells

or wells that contain more than one well screen interval. A reported tritium-helium age is the apparent age for the tritiated portion of the mixed-age groundwater. Groundwater ages can be further obfuscated by the existence of terrigenic ^{3}He sources. The $^{3}He/^{4}He$ ratio is measured along with the ^{4}He concentration to calculate the total ^{3}He. The $^{3}He/^{4}He$ ratio of radiogenic helium is estimated to be $2x10^{-8}$ (Saar et al., 2005; Torgersen, 1980). This conservative estimate is a typical $^{3}He/^{4}He$ ratio measured for radiogenic helium, but on the low side of the range of measured values. The $^{3}He/^{4}He$ ratio of mantle helium is between 6 to10 times the atmospheric $^{3}He/^{4}He$ ratio (Craig, 1978), but the concentration of mantle helium is also spatially variable. Mantle helium has been observed in groundwaters adjacent to faulting and in areas of magmatic activity (James et al., 2000; Kennedy, 1997; Moran et al., 2005). The addition of mantle helium makes it difficult to separate the tritiogenic helium from the other sources, because the contributions of radiogenic and mantle helium are unknown.

RESULTS

Noble gas and tritium data

Dissolved noble gas and tritium concentrations for Martis Valley groundwater samples are shown in Table 1. Noble gas concentrations are used to calculate groundwater recharge temperatures and excess air concentrations, and apparent groundwater ages are calculated using the tritium-helium method, as described in the previous section. These derived parameters are shown in Table 2. Differing results from the same wells during winter (December 2011-January 2012), summer (June 2012), and

fall (September 2012) sampling events reflect the extent of seasonal variation in the sources of groundwater produced in the Martis Valley basin. Additional samples were taken at local springs in late October 2012, including the headwaters of Middle Martis Creek (Z), a spring flowing into the Truckee River upstream of Martis Valley (X), and a spring flowing nearby the recently discovered and seismically active Polaris Fault (Y).

Table 1: Measured concentrations of tritium and dissolved noble gases.

ID	Collection Date	^{3}H (pCi/L)	err^{3}H (pCi/L)	$^{3}He/^{4}He$	err$^{3}He/^{4}He$	He (cc/g)	errHe (cc/g)	Ne (cc/g)	errNe (cc/g)	Ar (cc/g)	errAr (cc/g)	Kr (cc/g)	errKr (cc/g)	Xe (cc/g)	errXe (cc/g)
K	12/19/2011	0.14	0.34	3.00E-06	4.87E-08	2.32E-07	4.64E-09	3.45E-07	6.90E-09	4.25E-04	8.50E-06	8.85E-08	2.66E-09	1.24E-08	3.72E-10
O	12/19/2011	5.99	0.48	2.12E-06	1.84E-08	6.59E-08	1.32E-09	2.02E-07	4.09E-09	3.52E-04	7.04E-06	8.19E-08	2.46E-09	1.23E-08	3.68E-10
N	12/19/2011	5.22	0.51	1.34E-06	1.31E-08	5.13E-08	1.03E-09	2.38E-07	5.18E-09	3.69E-04	7.38E-06	8.67E-08	2.60E-09	1.28E-08	3.83E-10
L	12/20/2011	0.55	0.52	1.38E-06	1.35E-08	6.07E-08	1.21E-09	2.11E-07	4.59E-09	3.64E-04	7.28E-06	8.39E-08	2.52E-09	1.27E-08	3.80E-10
M	12/20/2011	0.31	0.39	4.01E-06	6.51E-08	2.82E-07	5.63E-09	1.94E-07	3.88E-09	3.29E-04	6.58E-06	7.80E-08	2.34E-09	1.18E-08	3.53E-10
E	1/19/2012	3.14	0.56	2.63E-06	1.97E-08	2.58E-06	5.17E-08	1.87E-07	6.07E-09	3.41E-04	6.83E-06	8.18E-08	2.45E-09	1.19E-08	3.58E-10
G	1/19/2012	5.70	0.64	3.10E-06	2.74E-08	4.07E-07	8.13E-09	1.97E-07	6.39E-09	3.45E-04	6.90E-06	7.98E-08	2.40E-09	1.16E-08	3.49E-10
C	1/19/2012	2.15	0.52	2.00E-06	3.45E-08	7.72E-08	1.54E-09	2.42E-07	5.87E-09	3.74E-04	7.47E-06	8.60E-08	2.58E-09	1.37E-08	4.12E-10
H	1/19/2012	4.26	0.57	2.73E-06	4.65E-08	1.68E-07	3.35E-09	2.85E-07	9.24E-09	3.95E-04	7.90E-06	8.51E-08	2.55E-09	1.20E-08	3.59E-10
D	1/19/2012	2.74	1.00	2.08E-06	1.58E-08	5.75E-08	1.15E-09	2.17E-07	4.33E-09	3.58E-04	7.17E-06	8.38E-08	2.51E-09	1.22E-08	3.67E-10
A	6/19/2012	2.51	0.50	3.33E-06	3.72E-08	4.76E-07	9.51E-09	1.97E-07	3.93E-09	3.48E-04	6.97E-06	7.99E-08	2.40E-09	1.21E-08	3.63E-10
B	6/19/2012	3.69	0.58	3.50E-06	5.00E-08	4.98E-06	9.96E-08	4.31E-07	8.62E-09	4.87E-04	9.75E-06	9.86E-08	2.96E-09	1.35E-08	4.04E-10
C	6/19/2012	2.05	0.34	2.39E-06	1.79E-08	1.15E-07	2.29E-09	2.35E-07	4.71E-09	3.72E-04	7.45E-06	8.40E-08	2.52E-09	1.21E-08	3.63E-10
D	6/19/2012	3.28	0.96	3.15E-06	2.37E-08	7.72E-07	1.54E-08	3.49E-07	6.98E-09	4.33E-04	8.66E-06	9.40E-08	2.82E-09	1.28E-08	3.83E-10
E	6/19/2012	2.50	0.50	2.75E-06	2.06E-08	3.46E-06	6.92E-08	2.08E-07	4.15E-09	3.53E-04	7.06E-06	8.05E-08	2.42E-09	1.17E-08	3.50E-10
F	6/19/2012	7.08	1.69	2.01E-06	1.50E-08	6.24E-08	1.25E-09	1.92E-07	3.84E-09	3.47E-04	6.94E-06	8.42E-08	2.52E-09	1.15E-08	3.44E-10
G	6/19/2012	4.20	0.52	3.22E-06	3.20E-08	4.40E-07	8.80E-09	1.98E-07	3.96E-09	3.52E-04	7.03E-06	8.28E-08	2.48E-09	1.15E-08	3.45E-10
H	6/19/2012	2.87	0.49	2.56E-06	3.72E-08	2.83E-07	5.65E-09	5.14E-07	1.03E-08	5.50E-04	1.10E-05	1.10E-07	3.30E-09	1.36E-08	4.09E-10
I	6/20/2012	11.69	0.77	1.73E-06	4.14E-08	5.69E-08	1.14E-09	2.04E-07	4.07E-09	3.45E-04	6.89E-06	7.85E-08	2.35E-09	1.23E-08	3.68E-10
J	6/20/2012	11.92	0.51	1.36E-06	3.25E-08	3.62E-08	7.23E-10	1.64E-07	3.28E-09	3.31E-04	6.63E-06	7.95E-08	2.38E-09	1.23E-08	3.68E-10
K	6/20/2012	-0.37	0.44	3.12E-06	4.94E-08	2.33E-07	4.66E-09	3.24E-07	6.47E-09	4.13E-04	8.25E-06	8.67E-08	2.60E-09	1.23E-08	3.70E-10
L	6/20/2012	0.16	0.27	1.34E-06	3.21E-08	4.63E-08	9.25E-10	2.00E-07	4.00E-09	3.52E-04	7.04E-06	8.08E-08	2.42E-09	1.21E-08	3.63E-10
M	6/20/2012	-0.32	0.55	4.02E-06	4.42E-08	3.26E-07	6.51E-09	1.89E-07	3.79E-09	3.40E-04	6.81E-06	7.75E-08	2.32E-09	1.11E-08	3.33E-10
N	6/20/2012	4.06	0.25	2.95E-06	2.21E-08	1.26E-07	2.52E-09	2.22E-07	4.44E-09	3.66E-04	7.33E-06	8.28E-08	2.48E-09	1.29E-08	3.87E-10
O	6/20/2012	5.23	0.42	2.07E-06	1.55E-08	6.63E-08	1.33E-09	2.14E-07	4.29E-09	3.62E-04	7.24E-06	8.21E-08	2.46E-09	1.29E-08	3.87E-10
A	9/5/2012	1.77	0.75	3.33E-06	4.61E-08	4.45E-07	8.89E-09	2.03E-07	4.07E-09	3.49E-04	6.98E-06	8.05E-08	2.42E-09	1.21E-08	3.64E-10
C	9/5/2012	1.42	0.43	2.79E-06	4.25E-08	1.59E-07	3.17E-09	2.31E-07	4.61E-09	3.69E-04	7.37E-06	8.47E-08	2.54E-09	1.18E-08	3.54E-10
B	9/5/2012	-0.50	0.85	3.48E-06	5.50E-08	4.27E-06	8.55E-08	3.02E-07	6.05E-09	4.10E-04	8.21E-06	9.01E-08	2.70E-09	1.28E-08	3.84E-10
D	9/5/2012	3.66	0.25	3.19E-06	4.42E-08	5.57E-07	1.11E-08	2.02E-07	4.04E-09	3.52E-04	7.04E-06	8.35E-08	2.51E-09	1.28E-08	3.84E-10
E	9/5/2012	2.36	0.40	2.61E-06	6.40E-08	2.27E-06	4.54E-08	1.98E-07	3.96E-09	3.50E-04	6.99E-06	8.34E-08	2.50E-09	1.24E-08	3.72E-10
F	9/5/2012	8.93	0.52	1.77E-06	2.18E-08	5.48E-08	1.10E-09	1.98E-07	3.97E-09	3.52E-04	7.03E-06	8.50E-08	2.55E-09	1.27E-08	3.80E-10
H	9/5/2012	2.14	0.79	2.27E-06	3.99E-08	2.46E-07	4.92E-09	6.62E-07	1.32E-08	7.48E-04	1.50E-05	1.33E-07	3.99E-09	1.72E-08	5.16E-10
G	9/5/2012	4.48	0.40	3.05E-06	4.43E-08	2.69E-07	5.38E-09	2.10E-07	4.21E-09	3.60E-04	7.19E-06	8.55E-08	2.57E-09	1.27E-08	3.81E-10
I	9/5/2012	10.44	0.54	1.65E-06	2.03E-08	5.64E-08	1.13E-09	1.99E-07	3.98E-09	3.18E-04	6.37E-06	7.40E-08	2.22E-09	1.04E-08	3.11E-10
N	9/6/2012	4.73	2.31	2.87E-06	3.53E-08	1.19E-07	2.38E-09	2.21E-07	4.43E-09	3.68E-04	7.36E-06	8.61E-08	2.58E-09	1.30E-08	3.90E-10
O	9/6/2012	2.39	2.25	2.93E-06	3.60E-08	1.19E-07	2.38E-09	2.12E-07	4.23E-09	3.60E-04	7.20E-06	8.42E-08	2.53E-09	1.18E-08	3.55E-10
K	9/6/2012	0.31	0.76	3.10E-06	4.33E-08	2.14E-07	4.29E-09	3.30E-07	6.59E-09	4.13E-04	8.25E-06	8.74E-08	2.62E-09	1.22E-08	3.65E-10
X	10/29/2012	9.72	0.57	1.45E-06	2.69E-08	3.88E-08	7.76E-10	1.79E-07	3.57E-09	3.41E-04	6.83E-06	8.30E-08	2.49E-09	1.22E-08	3.66E-10
Y	10/29/2012	-0.28	0.85	3.70E-06	6.84E-08	1.71E-07	3.41E-09	1.81E-07	3.62E-09	3.29E-04	6.57E-06	7.56E-08	2.27E-09	1.15E-08	3.44E-10
Z	10/29/2012	7.89	0.39	1.56E-06	2.88E-08	3.74E-08	7.47E-10	1.74E-07	3.49E-09	3.45E-04	6.91E-06	8.55E-08	2.57E-09	1.37E-08	4.12E-10

Table 2: Noble gas/tritium derived parameters

(recharge temperature, excess air concentration, and groundwater age).

ID	Collection Date	Well Type	Elevation (m asl)	Screen Begin/End (m below surface)		Frac Model*	Recharge Temp (°C)	Excess Air (cc/kg)	ΔNe %	^{3}H-^{3}He Age (yr)	+- (yr)	^{4}He rad (cm3STP/g)	+- (cm3STP/g)	Flow Depth (m)	Comments
K	12/19/2011	Production	1783	66	244	UA	7.65	9.89	108%	>50		1.42E-07	1.55E-06	419	
O	12/19/2011	Production	1830	43	274	UA	6.57	1.92	21%	Mantle He		1.80E-08	2.16E-07	67	
N	12/19/2011	Production	1832	46	274	UA	6.01	3.78	42%	Mantle He		0.00E+00	4.98E-07	59	
L	12/20/2011	Test Well	1783	20	81	UA	5.94	2.30	25%	>50		1.06E-08	2.67E-07	171	
M	12/20/2011	Test Well	1786	70	239	UA	8.43	1.55	18%	>50		2.36E-07	1.65E-07	137	
E	1/19/2012	Production	1823	38	183	UA	6.88	1.09	12%	Mantle He		2.54E-06	1.40E-07	332	
G	1/19/2012	Production	1770	87	283	UA	7.78	1.71	19%	Mantle He		3.60E-07	1.74E-07	153	
C	1/19/2012	Production	1820	140	415	UA	5.21	3.82	43%	Mantle He		1.90E-08	4.77E-07	262	
H	1/19/2012	Production	1796	30	313	CE	8.39	10.45	73%	Mantle He		9.70E-08	9.23E-07	69	
D	1/19/2012	Production	1783	85	338	UA	6.77	2.67	29%	Mantle He		5.57E-09	3.16E-07	142	
A	6/19/2012	Production	1753	82	274	UA	7.23	1.60	17%	Mantle He		4.29E-07	1.67E-07	206	
B	6/19/2012	Irrigation	1796	76	274	CE	6.57	17.95	157%	Mantle He		4.87E-06	2.56E-06	311	bubbles exsolving
C	6/19/2012	Production	1820	140	415	UA	6.80	3.79	41%	Mantle He		5.69E-08	4.65E-07	206	
D	6/19/2012	Production	1783	85	338	UA	6.43	9.98	107%	Mantle He		6.82E-07	1.60E-06	208	
E	6/19/2012	Production	1823	38	183	UA	7.51	2.34	25%	Mantle He		3.41E-06	2.64E-07	304	bubbles exsolving
F	6/19/2012	Production	1791	27	122	PR	12.30	54.31	31%	47	7	2.50E-08	1.39E-07	-182	
G	6/19/2012	Production	1770	87	283	PR	9.64	17.20	18%	Mantle He		4.01E-07	1.77E-07	64	
H	6/19/2012	Production	1796	30	313	PR	9.19	40.51	21%	Mantle He		1.95E-07	3.56E-06	43	
I	6/20/2012	Irrigation	1797	15	61	UA	7.46	2.01	22%	27	2	8.57E-09	2.26E-07	127	
J	6/20/2012	Cistern	2073	NA	NA	UA	5.62	0.00	0%	0		0.00E+00	1.71E-09	-25	open to atmosphere
K	6/20/2012	Production	1783	66	244	UA	7.70	8.70	95%	>50		1.50E-07	1.34E-06	379	bubbles exsolving
L	6/20/2012	Test Well	1783	20	81	UA	6.97	1.80	20%	>50		0.00E+00	1.93E-07	141	sampled with bailer
M	6/20/2012	Test Well	1786	70	239	CE	9.62	21.68	16%	>50		2.82E-07	1.25E-07	159	Under contruction, no pump, not purged
N	6/20/2012	Production	1832	46	274	UA	5.91	2.92	32%	Mantle He		7.29E-08	3.58E-07	99	
O	6/20/2012	Production	1830	43	274	UA	5.96	2.51	27%	Mantle He		1.52E-08	3.01E-07	90	
A	9/5/2012	Production	1753	82	274	UA	7.31	1.96	21%	Mantle He		3.96E-07	1.93E-07	233	
C	9/5/2012	Production	1820	140	415	PR	8.18	8.82	40%	Mantle He		1.13E-07	4.16E-07	179	
B	9/5/2012	Irrigation	1796	76	274	UA	6.13	7.37	79%	>50		4.20E-06	1.04E-06	386	
D	9/5/2012	Production	1783	85	338	UA	6.04	1.75	19%	Mantle He		5.09E-07	1.70E-07	243	
E	9/5/2012	Production	1823	38	183	UA	6.27	1.64	18%	Mantle He		2.22E-06	1.58E-07	382	
F	9/5/2012	Production	1791	27	122	UA	5.87	1.57	17%	32	2	8.44E-09	1.44E-07	99	
H	9/5/2012	Production	1796	30	313	CE	4.79	58.71	287%	Mantle He		8.24E-08	4.72E-06	283	
G	9/5/2012	Production	1770	87	283	UA	5.90	2.21	24%	Mantle He		2.19E-07	2.23E-07	217	
I	9/5/2012	Irrigation	1797	15	61	UA	11.16	2.10	24%	26	2	8.24E-09	2.30E-07	103	
N	9/6/2012	Production	1832	46	274	UA	5.37	2.83	31%	Mantle He		6.62E-08	3.06E-07	137	
O	9/6/2012	Production	1830	43	274	UA	6.72	2.49	27%	Mantle He		6.80E-08	2.51E-07	93	
K	9/6/2012	Production	1783	66	244	UA	7.98	9.05	99%	>50		1.29E-07	1.40E-06	411	
X	10/29/2012	Spring	1939	N/A	N/A	UA	5.79	0.67	7%	1	2	0.00E+00	3.62E-08		spring sample, possible gas loss
Y	10/29/2012	Spring	1819	N/A	N/A	UA	8.46	0.91	10%	>50		1.28E-07	6.67E-08		spring sample, possible gas loss
Z	10/29/2012	Spring	2221	N/A	N/A	UA	2.99	0.42	5%	11	1	0.00E+00	1.38E-08		spring sample, possible gas loss

*Fractionation Models include UA-unfractionated air, PR-partial re-equilibration, and CE-closed equilibrium.

Most of the wells available for sampling in Martis Valley are production wells. Well locations are show in Figure 7. Many of these production wells have long well screens and/or multiple well screen intervals as shown in Figure 8. Long, alternating perforated intervals allow high production rates in Martis Valley's complex hydrogeological setting with variable layering of permeable and semi-permeable

volcanic, glacial, and alluvial deposits (Fram et al., 2009). These complex well screen intervals also produce mixed groundwater samples, with varying sources and residence times.

Figure 7: Letter labels show the locations of the sampled production well locations in Martis Valley. Also shown is the location of the cross section shown in Figure 8.

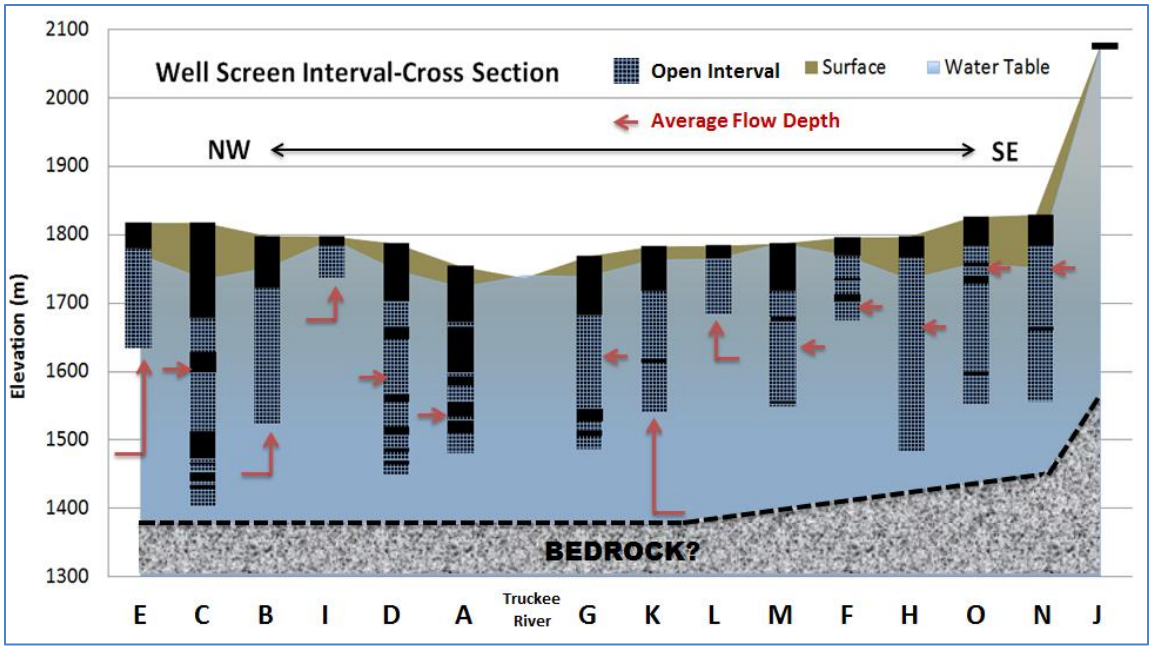

Figure 8: Schematic cross section showing well screen intervals, calculated average flow depth, and the water table. All wells are projected onto the cross section. Depth to bedrock is approximate and based on the maximum reported depth (Fram et al., 2009). Depth to bedrock is likely shallower beneath higher elevation wells.

Tritium in Martis Valley

Tritium concentrations measured in surface water in the Truckee River and Donner Creek were 11.81 (±0.86) pCi/L and 11.59 (±0.75) pCi/L respectively. These tritium concentrations are consistent with previous GAMA studies of California surface waters that are in exchange with present-day, atmospheric tritium. A lower tritium concentration of 8.38 (±1.58) pCi/L was found in Martis Creek. Spring X is located at the headwaters of Middle Martis Creek and had a tritium concentration of 7.89 (±0.39) pCi/L and a tritium/helium-3 age of 11 years. Lower tritium levels in Martis Creek compared to

Truckee River and Donner Creek suggest that a significant source of water for Martis Creek is discharging groundwater.

The wells listed as having tritium/helium-3 ages ">50 years" in Table 2 contained <1 pCi/L of tritium. Wells containing >1 pCi/L of tritium labeled as "mantle He" in Table 2 have average ages <50 years, but exact ages cannot be determined due to the presence of mantle helium, as explained below. Still, the presence of tritium in most groundwater samples from Martis Valley provides important evidence for the pervasive presence of recent recharge in produced groundwater. It is likely that some >50 year old water is mixed in when tritium is <12 pCi/L. Lower concentrations of Tritium were found during the September sampling than the June or Winter sampling events for wells A, B, C, E, H, and O. This possibly suggests that these wells rely on a younger groundwater source for a portion of their total output, which becomes more depleted after a dry summer of pumping.

One sample (Sample J from a high-elevation cistern) had a zero tritium/helium-3 age and a tritium activity of 11.9±0.5 pCi/L. A zero tritium/helium-3 age is calculated when no tritiogenic helium-3 is detected and can be caused by re-equilibration of dissolved gases in the groundwater sample with atmospheric gases before or during sample collection (from insufficient well purging or a sampling environment that allows exposure to atmospheric gases). The cistern from which sample J was collected has a 1 m diameter opening exposed to the atmosphere, and the sample was collected without purging. The poor sampling environment for sample J make it likely that the true mean groundwater age is greater than the calculated two years and that the measured tritium

activity does not reflect current recharge at this site. The cistern, however, is located at a much higher elevation than the other wells sampled and the high measured tritium activity is consistent with a general pattern of higher tritium at higher elevation sites (Michel and Schroeder, 1994).

Water isotopic composition

Well and surface water samples were analyzed for $\delta^{18}O$ and $\delta^{2}H$ of the water molecule at CSUEB on a Los Gatos Research water isotope analyzer. Overall, samples are strongly enriched in the light isotopes, ^{1}H and ^{16}O, owing to the cold, high elevation source area for meteoric water in Martis Valley. Groundwater samples from Martis Valley produced isotopically lighter water than surface water samples, indicating the source of most groundwater recharge is precipitation/snowmelt. The surface water samples from Donner Creek and the Truckee River are isotopically heavier because they are released from Donner Lake and Lake Tahoe respectively. Water in the lakes is affected by evaporation, which shifts the water isotopic compositions to higher $\delta^{18}O$ and $\delta^{2}H$ values. The degree to which the waters are shifted to higher $\delta^{18}O$ and $\delta^{2}H$ values depends on the lake surface area, as well as the evaporation potential, humidity, inflow/outflow ratio, residence time, and the isotopic composition of the source of water vapor. Lake Tahoe water has a long 700 year residence time allowing for a significant amount of evaporation and isotopic fractionation to take place. Donner Lake produces a similar effect on Donner Creek water, but with less enrichment, given a likely much shorter residence time for Donner Lake water. Well I produced water with $\delta^{18}O$ and $\delta^{2}H$

values significantly higher than typical groundwater found in Martis Valley (Figure 9). Well I is in close proximity to Donner Creek, has a shallow screened interval beginning at a depth of 15 m below ground surface, and has a tritium concentration similar to local surface water. Well I is producing water from a mixture of sources possibly including surface water from Donner Creek and/or the quarries to the west of Well I, which would also likely experience evaporation.

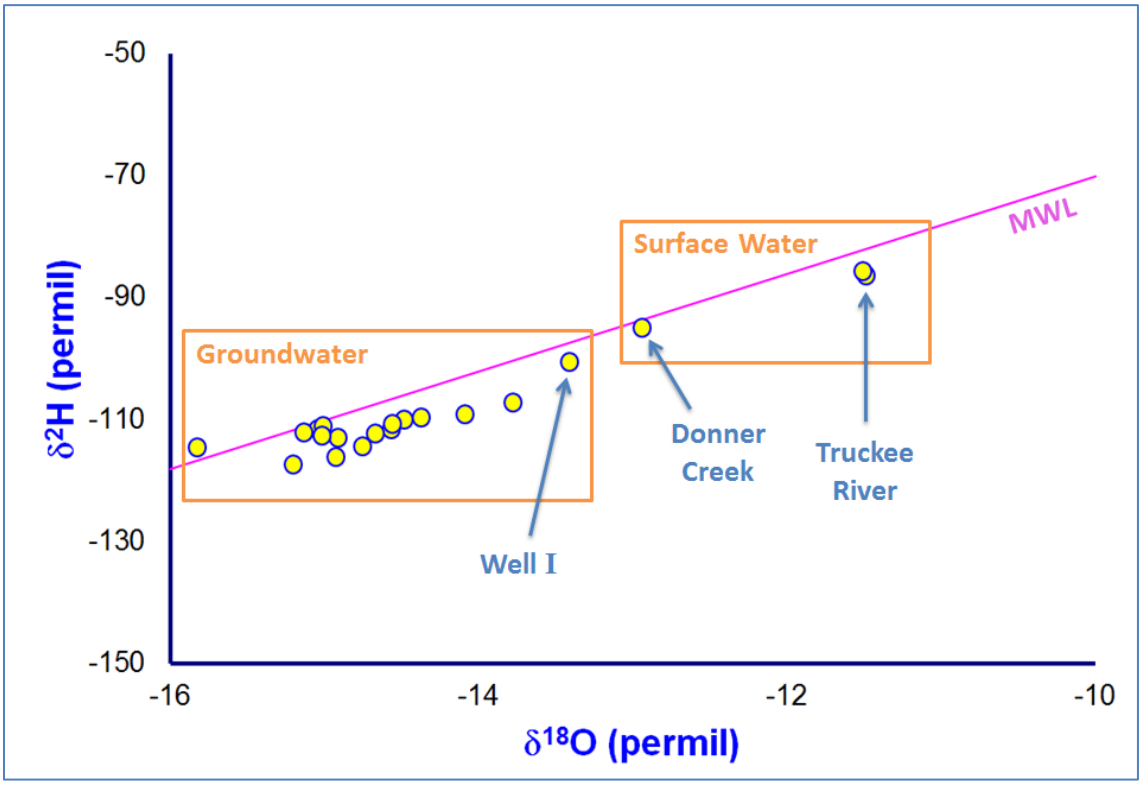

Figure 9: Isotopic composition of Martis Valley groundwater and surface water. Line labeled MWL (meteoric water line) depicts expected variations in isotopic composition of meteoric water. Similar isotopic compositions between surface water samples and well I reveal nearby Donner Creek as a possible surface water recharge source for well I.

Noble gas recharge temperatures

Figure 10 shows the calculated noble gas recharge temperatures in Martis Valley production wells averaged from each sampling. There is a general pattern of lower recharge temperatures with increasing altitude in the mountains and foothills surrounding Martis Valley, and recharge temperatures are highest for wells on the valley floor.

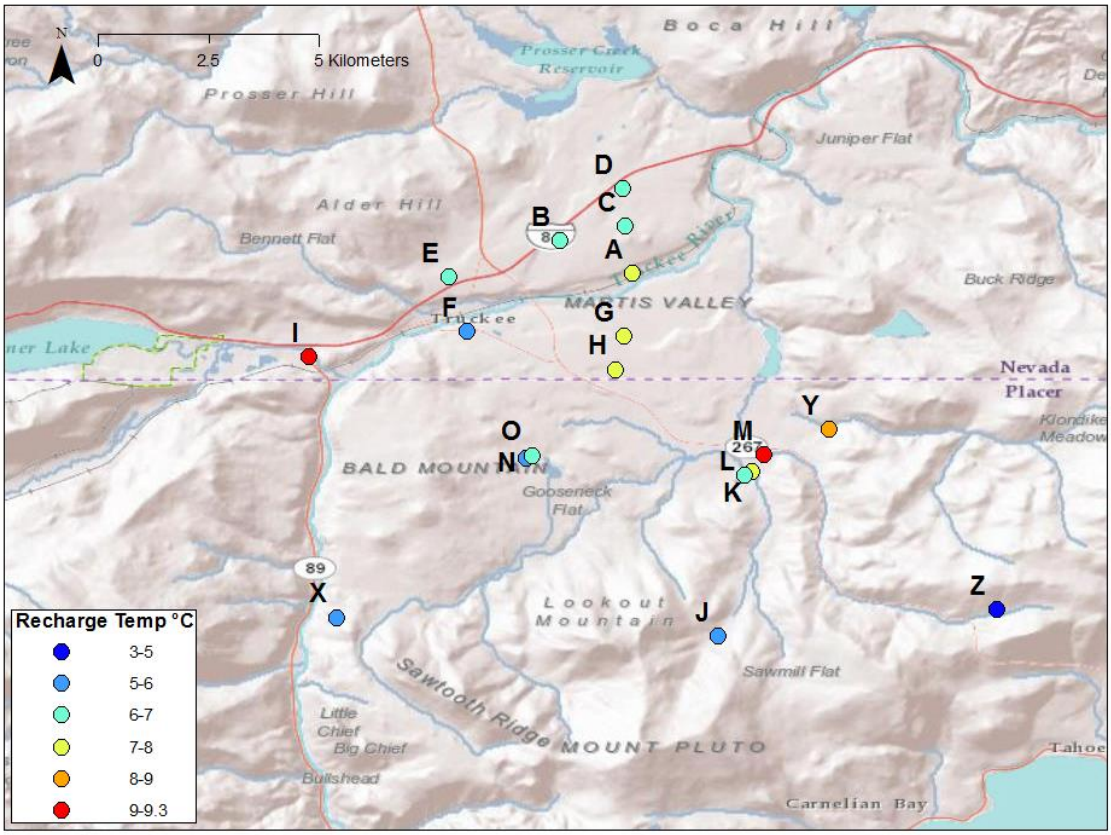

Figure 10: Well locations are shown with calculated noble gas recharge temperatures. Noble gas recharge temperatures tend to decrease with increasing altitude.

An anomalously high recharge temperature was found in the sample from Well I collected in September. This high recharge temperature is likely the result of mixing

between local groundwater and a component of water from nearby Donner Creek or the quarries to the west (see previous section). High recharge temperatures found at well M and spring Y were likely due to poor sampling conditions.

The likely source for most groundwater recharge in Martis Valley is snowmelt, which is released from the snowpack in spring. Calculated noble gas recharge temperatures range between 5 and 11°C, and are significantly higher than would be expected for direct infiltration of snowmelt. In most samples, groundwater discharge temperatures are significantly higher than noble gas recharge temperatures. These differences reflect both surface and soil processes and deeper subsurface processes. In the near-subsurface, water temperature increases as snowmelt equilibrates to temperatures in the vadose zone (at a temperature close to mean annual air temperature for that elevation) and eventually reaches the water table – these processes are reflected in the difference between the snow melting point and noble gas recharge temperature (the blue bar in Figure 11). During subsurface transport, groundwater temperature increases due to geothermal heating, with the magnitude of heating proportional to the depth of the flow path – this process is reflected in the difference between noble gas recharge temperature and well discharge temperature (the red bar in Figure 11).

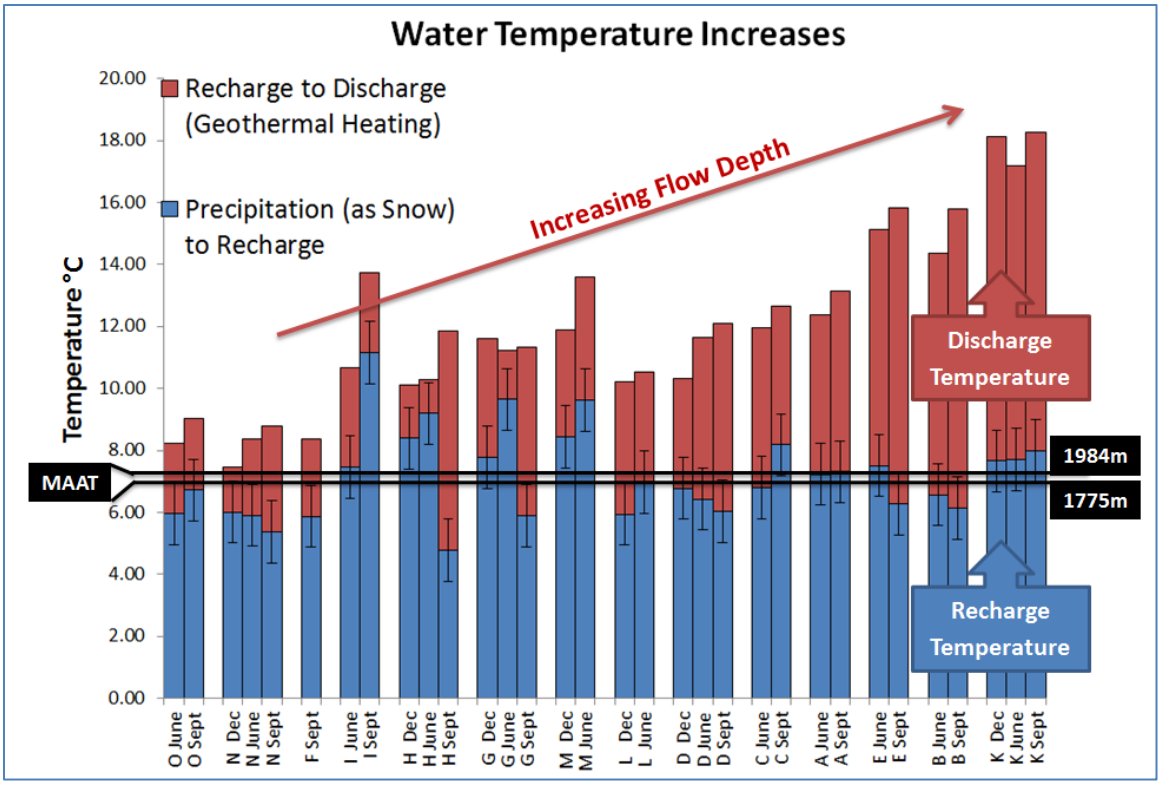

Figure 11: Discharge, recharge, and mean annual temperature for Martis Valley wells plotted in order of increasing flow depth. Recharge temperatures in Martis Valley are higher than expected for direct infiltration of snowmelt. Most recharge temperatures fall near the mean annual air temperatures at 1775m and 1984m elevations (NOAA NCDC, accessed February 2013; USDA NRCS, accessed February 2013), suggesting most recharge is occurring within a soil zone, at an altitude near these elevations.

Lower groundwater recharge temperatures found at higher well surface elevation sites such as Z, Y, and J are consistent with lower air temperatures at higher elevations – the standard adiabatic lapse rate is -6.5°C/km. However, historical air temperature data

from Martis Valley weather stations reveal a unique microclimate with a similar mean annual air temperature (MAAT) for the lower 200 meters of the valley. Cold air flows down the slopes of the valley causing somewhat anomalously low MAATs as these cool air masses pool on the valley floor. The Truckee Ranger Station at 1775 m elevation had a MAAT of 6.9°C between 1993 and 2008 (NOAA NCDC, accessed February 2013) while the Truckee #2 Snotel station at 1934 m elevation had a MAAT of 7.2°C between 1993 and 2008 (USDA NRCS, accessed February 2013). The adiabatic lapse rate would predict the Snotel site to be 1°C colder. The MAAT is representative of the temperature of the vadose zone below 2-3 m depth, which is nearly constant throughout the year (Flint et al., 2008). The typical thickness of the vadose zone for each well sampled was greater than 20 m, with the exception of Well I having a 4 m vadose zone. These vadose zones are thick enough to allow infiltrating snowmelt time to re-equilibrate at the MAAT. Most of the wells in Martis Valley had recharge temperatures similar to these two MAATs (Figure 11). These recharge temperatures are therefore higher than those expected for direct infiltration of snowmelt. Likewise, the recharge temperatures of the valley wells are higher than 6 degrees, the estimated MAAT at 2100 m, or about 330 m above the valley floor. This suggests that most groundwater sampled in this study originated as recharge that had thermally equilibrated within the vadose zone, and occurred at elevations within the lower 330 m of the watershed (Figure 12).

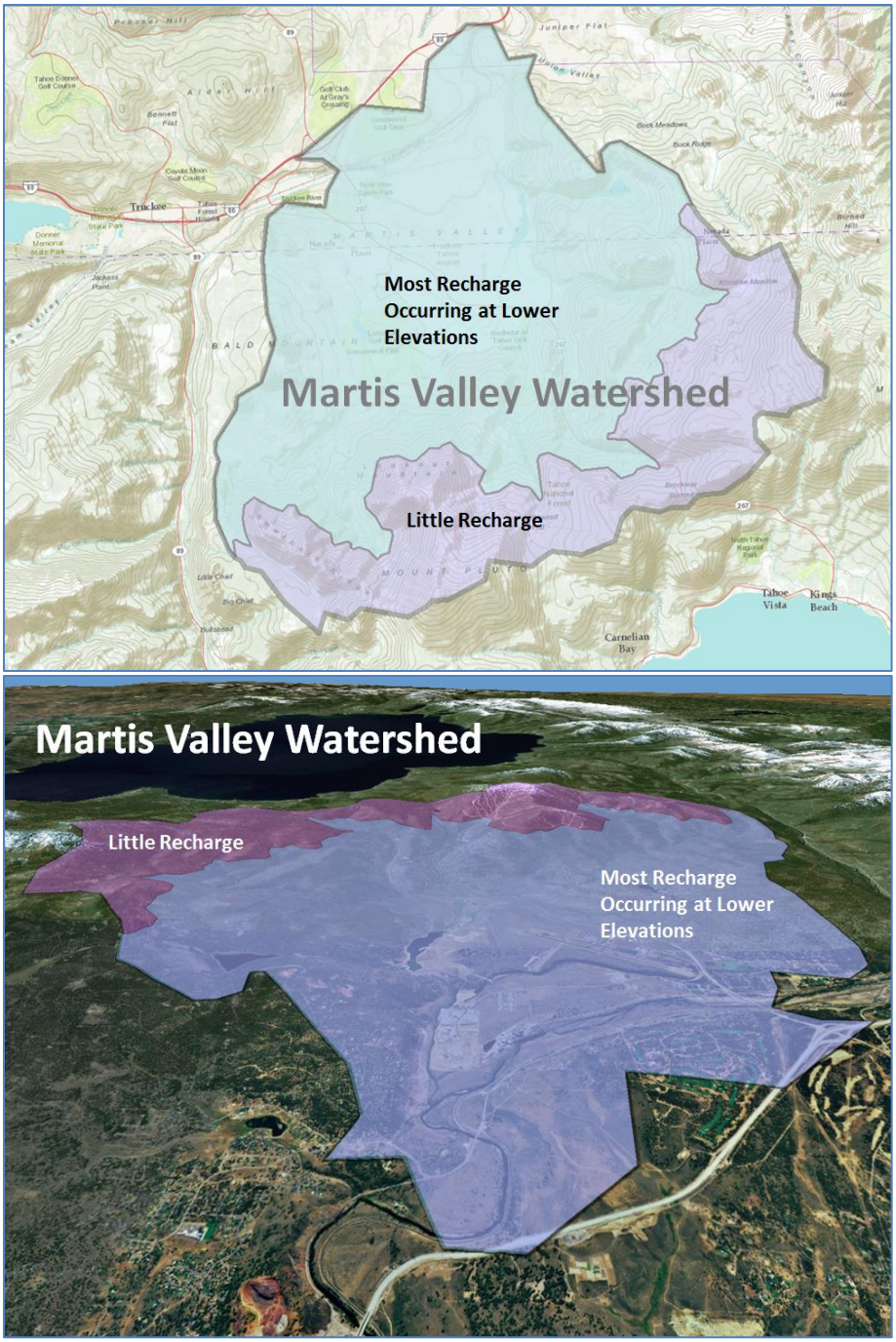

Figure 12: Maps showing the extent of the Martis Valley Watershed with recharge locations. Most recharge is occurring in the lower 330 m of the valley. Little recharge occurs in the higher elevations.

Wells in Figure 11 are plotted in order of increasing flow depth. Flow depth is the calculated depth that groundwater must have traveled to in order to increase its recharge temperature to its discharge temperature. A number of wells were sampled in winter, summer and fall to assess seasonal variability in tritium and recharge temperature. Wells with deeper flow depths had less seasonal variability (Figure 13). Seasonal variability in recharge temperature shows a weak correlation with flow depth. Differently aged groundwater sources can have a similar recharge temperature since most groundwater produced at these wells is recharging in the lower 330 m of the watershed at similar temperatures. For certain wells (e.g. wells M and H), partial degassing during sampling or in the wellbore may be responsible for seasonal variability in noble gas recharge temperature.

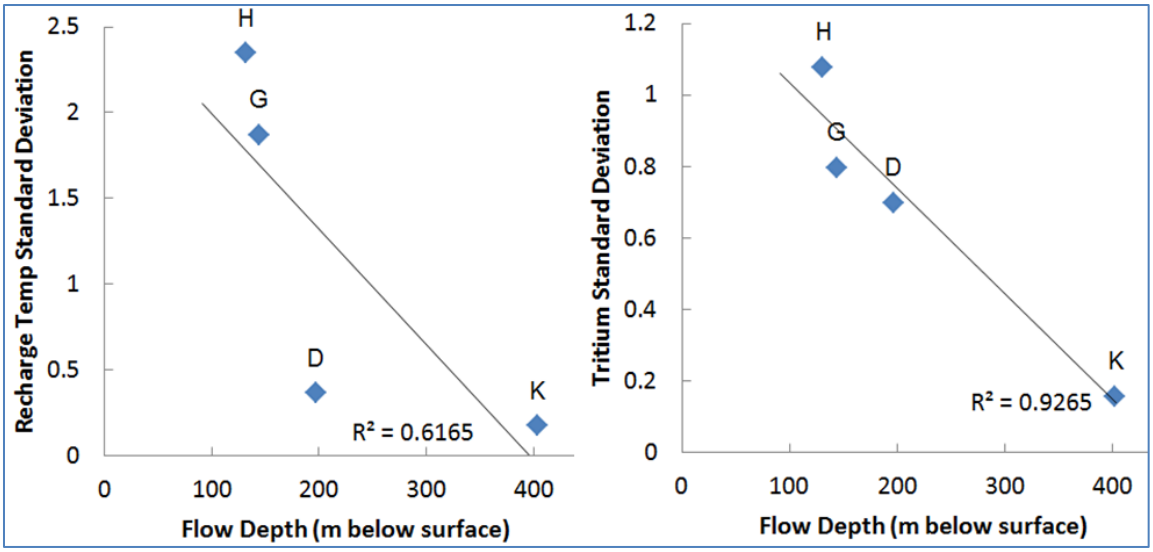

Figure 13: The variability of recharge temperatures and tritium for wells sampled three times (during winter, summer, and fall) decreases with increasing average flow depth (see text for explanation).

The thickness of groundwater bearing deposits in Martis Valley are estimated at up to 366m (Fram et al., 2009). Assuming a geothermal gradient of 25°C/km, groundwater flowing through the base of the water bearing deposits, and warming to the ambient temperature, should be 9°C warmer than groundwater near the surface. In the samples analyzed for this study, groundwater discharge temperatures are always greater than calculated noble gas recharge temperatures, by as much as 10 °C, an observation consistent with deep flow paths and warming during subsurface transport. An estimated average flow depth for each well was calculated by comparing the measured well discharge temperature to the calculated noble gas recharge temperature, and then determining the depth within the basin required to increase its recharge temperature to its

discharge temperature, assuming a geothermal gradient of 25°C/km. Martis Valley is located between the Sierra Nevada, which has a low geothermal gradient, and the higher heat flow Basin and Range region. The geothermal gradient for Martis Valley was estimated to be similar to the continental geothermal gradient of 25°C/km by comparing geothermal maps compiled by Southern Methodist University's Geothermal Lab (http://www.google.org/egs/, accessed March 2013).

Flow depths are shown on the cross section in Figure 8. Well K, one of the valley's most productive wells, has a calculated flow depth near the estimated maximum depth to bedrock. This well also has a groundwater age of greater than 50 years, as demonstrated by the absence of tritium, consistent with the long flow path and residence time inferred from the deep flow depth. The overall pattern is that the modeled mean flow depth generally increases towards the lower elevations of the valley floor. Electrical conductivity was likewise found to increase with increasing flow depths (Figure 14). This is expected since electrical conductivity is an indicator of dissolved solids, which tend to increase with longer flow paths and a longer time period for water-rock interaction.

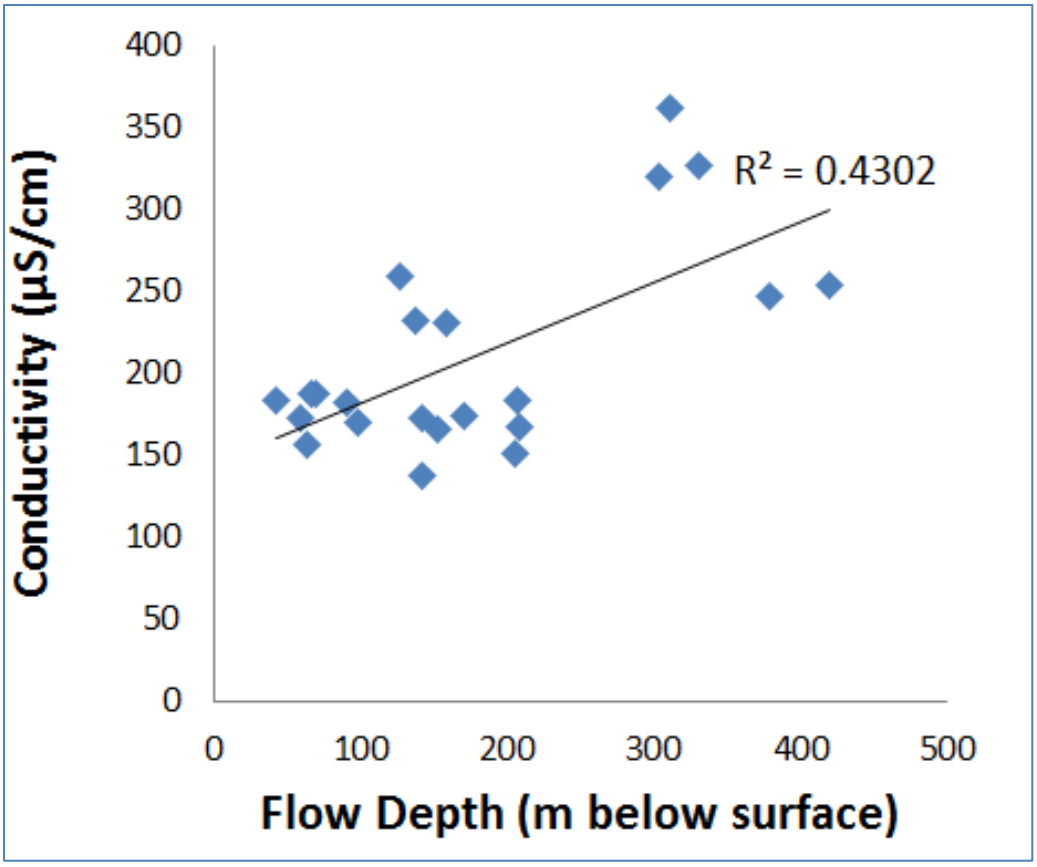

Figure 14: A positive correlation is observed between measured electrical conductivity and calculated mean flow depth.

Deeper flow depths suggest longer flow paths and older groundwater ages. Wells with shallower flow depths contain younger groundwater and higher average tritium concentrations (Figure 15). This suggests that differing amounts of younger water is likely the driver of seasonal groundwater variability. Wells sampling younger water (shallower flow paths) are more likely to change seasonally because they sample different flow depths at different times of the year. Wells H and G show the most variability in ^{3}H and recharge temperature. Most wells contained lower ^{3}H concentrations at the

September sampling, likely because the youngest water had been already been pumped from the well capture zone earlier in the year.

Tritium is a better indicator of seasonal variability in *groundwater source* than noble gas recharge temperatures (Figure 13) since different groundwater sources will have different flow paths to a given receptor and will have different tritium concentrations (from differences in both initial tritium at the time of recharge and in the amount of radioactive decay during transport along shorter or longer flow paths). Differences in tritium concentration likely reflect differences in mixing between younger and older groundwater in the well.

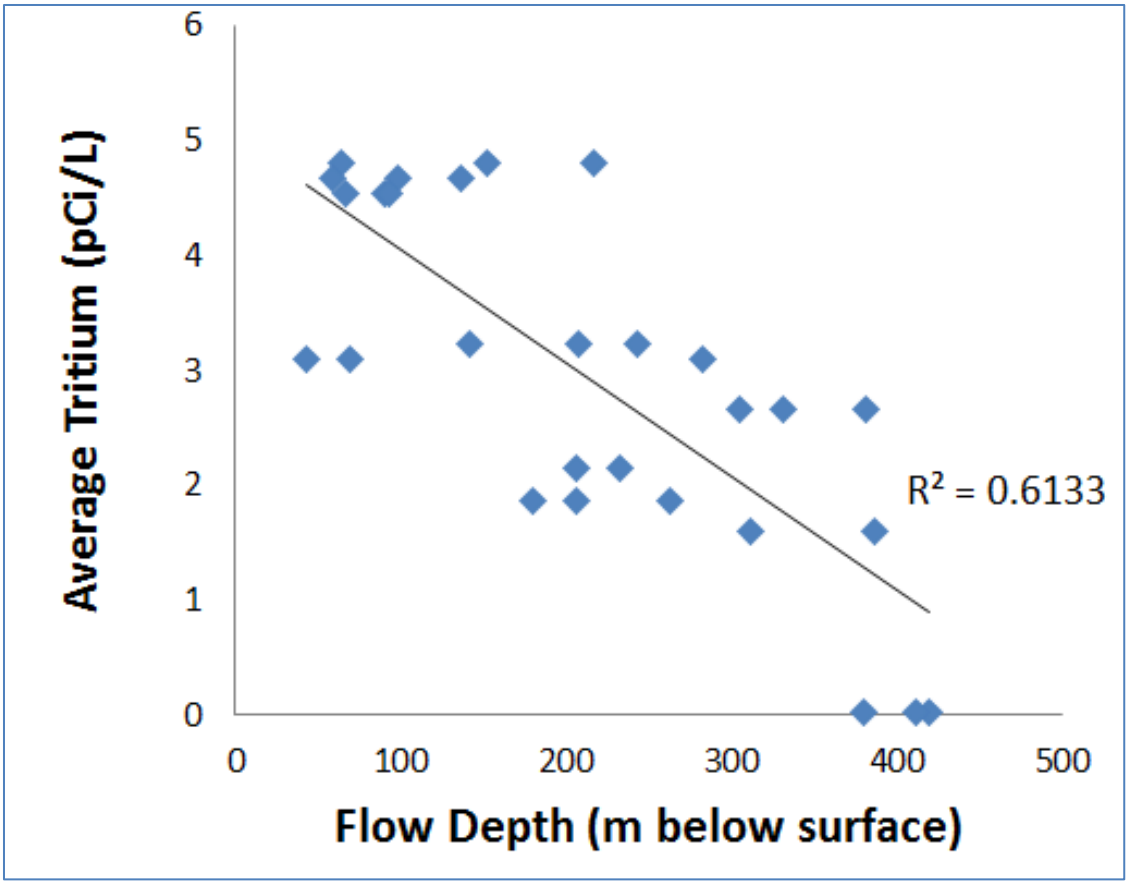

Figure 15: Wells with shallower estimated mean flow depth contain a younger groundwater component as inferred from higher average tritium concentrations, suggesting younger water is the likely the driver of seasonal groundwater variability.

Excess air and recharge mechanism

The concentration of excess air entrained during groundwater recharge gives an indication of the conditions under which recharge occurred. High levels of excess air (typically greater than 150% ΔNe) can be associated with mountain block recharge (Manning and Caine, 2007). This occurs at high elevations in alpine/sub-alpine settings where more bedrock is exposed and recharge occurs relatively rapidly with turbulent flow

into fractures. Low levels of excess air are typically associated with alluvial deposits and recharge via streams where recharge occurs more slowly or with minimal entrainment of air (Cey et al., 2009). Figure 16 shows generally low levels of excess air in Martis Valley groundwater compared to areas where mountain block recharge has been inferred based on excess air concentrations. This supports the interpretation of noble gas recharge temperatures indicating that recharge is occurring primarily at lower elevations in the valley floor's alluvial deposits.

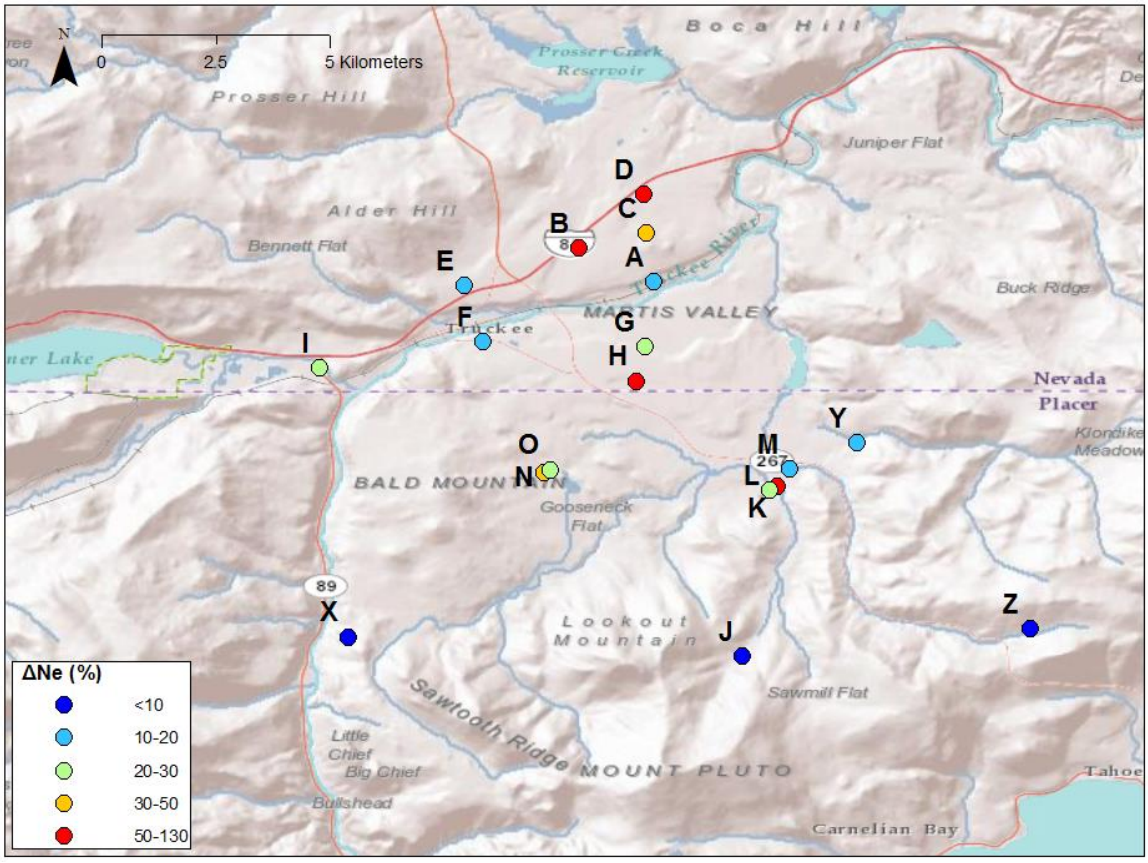

Figure 15: Relatively low excess air concentrations in Martis Valley suggest most recharge is occurring in the alluvial deposits within the valley floor.

Mantle helium in Martis Valley groundwaters

Many of the wells in Martis Valley have high helium concentrations and high $^{3}He/^{4}He$ ratios that would lead to calculations of erroneously high tritium-helium ages (samples labeled "mantle He" in Table 2). These waters have helium isotopic compositions that are too high in ^{3}He to be supported by the measured ^{3}H. In continental settings, mantle (also called magmatic) helium is transported to the earth's crust via conduits such as faults or other structures associated with regional tectonic activity and dissolves into groundwater. Helium concentrations in excess of what can be accounted for by dissolved atmospheric helium concentrations or entrained excess air can have either tritiogenic, radiogenic, or mantle helium sources. Equations 7 and 8 explain the different sources making up the total ^{3}He and ^{4}He in a groundwater sample.

An accurate determination of the tritiogenic ^{3}He concentration is needed in order to calculate a meaningful tritium-helium groundwater age. In most groundwaters, mantle helium is not present and the contribution to ^{3}He from radiogenic helium, which has a low $^{3}He/^{4}He$ of $2x10^{-8}$ (Torgersen, 1980) relative to the atmospheric ratio of $1.384x10^{-6}$, is small and can be accounted for. The presence of even small amounts of mantle helium, which has a $^{3}He/^{4}He$ ratio 6-10 times higher than the atmospheric ratio (Craig, 1978), makes it difficult to distinguish mantle ^{3}He from tritiogenic ^{3}He. A further complication is that while production of radiogenic helium can be assumed to be relatively uniform for a given basin, the spatial distribution of mantle helium can be highly heterogeneous.

In Martis Valley wells, many of the groundwater samples have high concentrations of helium compared to concentrations observed in a large number of wells

throughout the state (http://www.swrcb.ca.gov/gama/geotracker_gama.shtml). These concentrations are in excess of what could be accounted for by atmospheric solubility equilibrium or excess air. The source of excess helium can be examined by plotting helium isotopic composition against helium concentration, after correcting both for the excess air component (by subtracting excess air helium) and after normalizing groundwater helium concentration to equilibrium solubility helium concentration. In practice, one plots groundwater $^{3}He/^{4}He$ (corrected for excess air) against the ratio of equilibrium atmospheric ^{4}He concentration to groundwater ^{4}He concentration (corrected for excess air) (Saar et al., 2005). Such a plot for Martis Valley wells (Figure 17) shows that the excess helium in Martis Valley groundwater is composed of a mixture of mantle and radiogenic helium. On this plot, atmospheric helium plots at 1,1. Tritium decay increases the groundwater $^{3}He/^{4}He$ ratio but does not affect the ^{4}He concentration, and so moves the atmospheric value up parallel to the y-axis. Radiogenic production of helium in the crust moves groundwater helium to lower $^{3}He/^{4}He$ composition (since radiogenic helium has a lower ratio than the atmosphere). The y-intercept helium isotopic composition at zero equilibrium helium (i.e. atmospheric helium) for this mixing line is 0.015, the isotopic composition of radiogenic helium normalized to air. This intercept is based on a conservative estimate of the ratio of radiogenic helium $^{3}He/^{4}He$ of $2x10^{-8}$ (Saar et al., 2005).

The addition of mantle helium, which has a much higher $^{3}He/^{4}He$ ratio than air, moves groundwater helium to isotopic compositions higher than atmospheric and much higher than radiogenic helium. The y-intercept helium isotopic composition at mantle

helium is 8±2, i.e., the isotopic composition of mantle helium normalized to air (Craig, 1978). The presence of radiogenic and mantle helium in Martis Valley groundwater samples can be assessed by examining samples that have little or no tritiogenic helium, i.e. samples with tritium concentrations of <1 pCi/L and groundwater ages in excess of 50 years. In Figure 16, wells K,M, and Y plot on a mixing line (shown in red in Figure 17) with an intercept of 3.0, reflecting input of primarily mantle and radiogenic helium. The sources of excess helium for these samples were 35-40% mantle helium, and 60-65% radiogenic helium. Most wells in southern Martis Valley plotted along this red mixing line. Most wells in the northern Martis Valley plotted along a lower (blue in Figure 17) line, suggesting that less mantle helium is present in this area. There is a possible third mixing line (shown in dashed blue in Figure 17), for wells in northeast Martis Valley with a lower, but still significant, quantity of mantle helium. Determining the groundwater age of samples that plot along these lines is difficult because the calculation of tritiogenic helium is highly sensitive to small differences in both the concentration and isotopic composition of the estimated mantle + radiogenic (i.e., terrigenic) helium component.

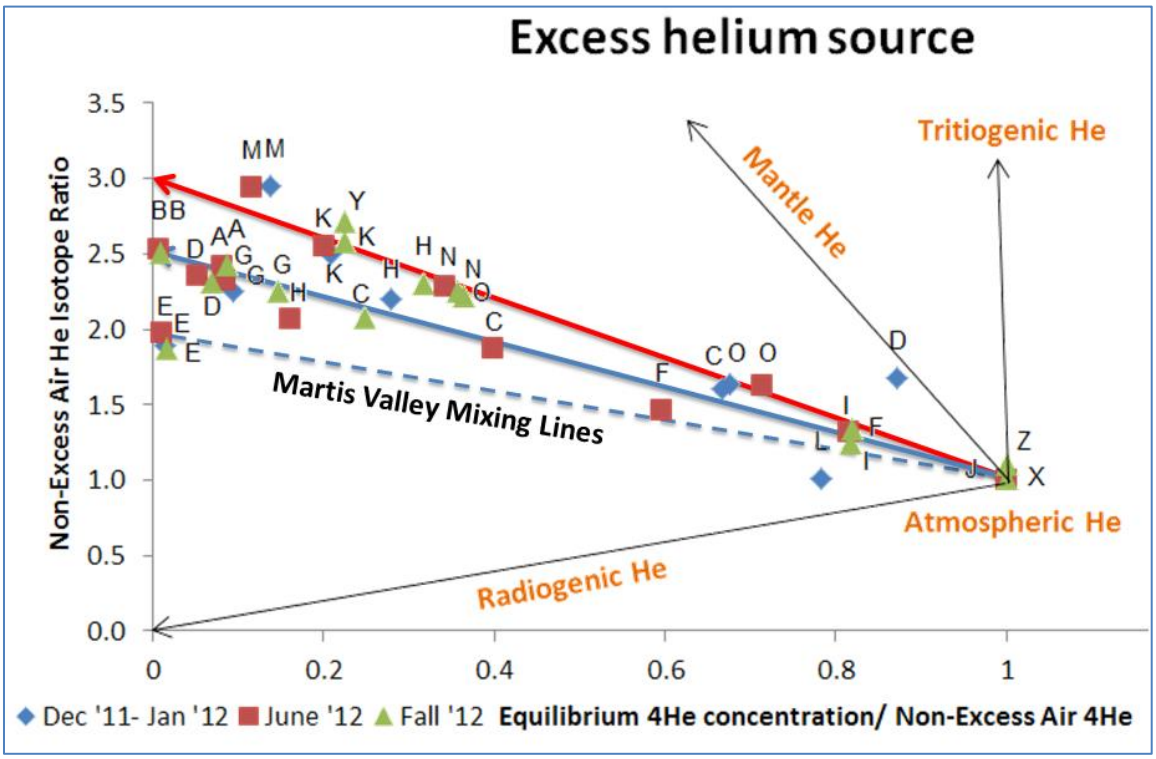

Figure 17: By plotting the equilibrium ^{4}He concentration/ non-excess air ^{4}He versus the non-excess air $^{3}He/^{4}He$ ratio to atmospheric $^{3}He/^{4}He$, the source of excess helium in Martis Valley is identified as a mixture of mantle and radiogenic helium. The proportions of these mixtures vary spatially. Wells in southern Martis Valley, containing 35-40% mantle helium, plot along the red mixing line. Wells in northern and northeastern Martis Valley contain less mantle helium and plot along the blue and dashed-blue mixing lines. The position along the mixing line gives a rough indication of the groundwater's age. Younger samples plot closer to the atmospheric He end member and older samples plot towards the Y intercept.

Sources of mantle helium are generally deep-seated, so flow paths require conduits that bring deep water into shallower systems, a process that can produce groundwaters with mixed ages. The concentration of terrigenic (mantle + radiogenic) helium can be used to identify very old water components, i.e. samples with concentrations of terrigenic ^{4}He in excess of 50% of atmospheric concentrations are assumed to contain a portion of groundwater that is greater than 1000 years old (Torgersen, 1980). The accumulation rate of radiogenic 4He depends on the ratio of radiogenic helium $^{3}He/^{4}He$, the concentrations of Uranium and Thorium found in the sediment, and the porosity of the aquifer. The 1000 year old figure assumes a ratio of radiogenic helium $^{3}He/^{4}He$ of $2x10^{-8}$, average Uranium and Thorium concentrations, and average porosity. Tritium can be used to identify very young groundwater - groundwater samples with tritium concentrations of greater than 1 pCi/L contain a portion of groundwater that is less than 50 years old. Plotting terrigenic ^{4}He versus tritium concentrations (Figure 18) shows whether the groundwater is young, intermediate, old or mixed age. Groundwater age classifications are explained in Table 3.

Table 3: Groundwater Age Classification

Classification	**Age range**	**Tritium?**	**Terrigenic He?**	**Number of samples**
Young	<50 years	Yes (>1 pCi/L)	Low (<50% excess He)	10
Intermediate-age	50-1000 years	No (<1 pCi/L)	Low (<50% excess He)	1
Old	>1000 years	No (<1 pCi/L)	High (>50% excess He)	7
Mixed-age	mixed	Yes (>1 pCi/L)	High (>50% excess He)	20

Most of the wells in Martis Valley produce groundwater with a mixed age (Figure 18). This is expected in wells with long and multiple well screen intervals. The degree of mixing between the three age groups is indicated by where a value plots in the mixed-age section of the graph. Many of the wells sampled during multiple sampling events showed a seasonal variation in the proportions of different groundwater sources that compose their mixed groundwater age. Wells D, G, H, and C had significant changes in groundwater source mixing between winter and summer. Wells B, O, F, and I had significant changes in groundwater source mixing between summer and fall. The wells with the most groundwater source seasonal variability generally had shallower average flow depths

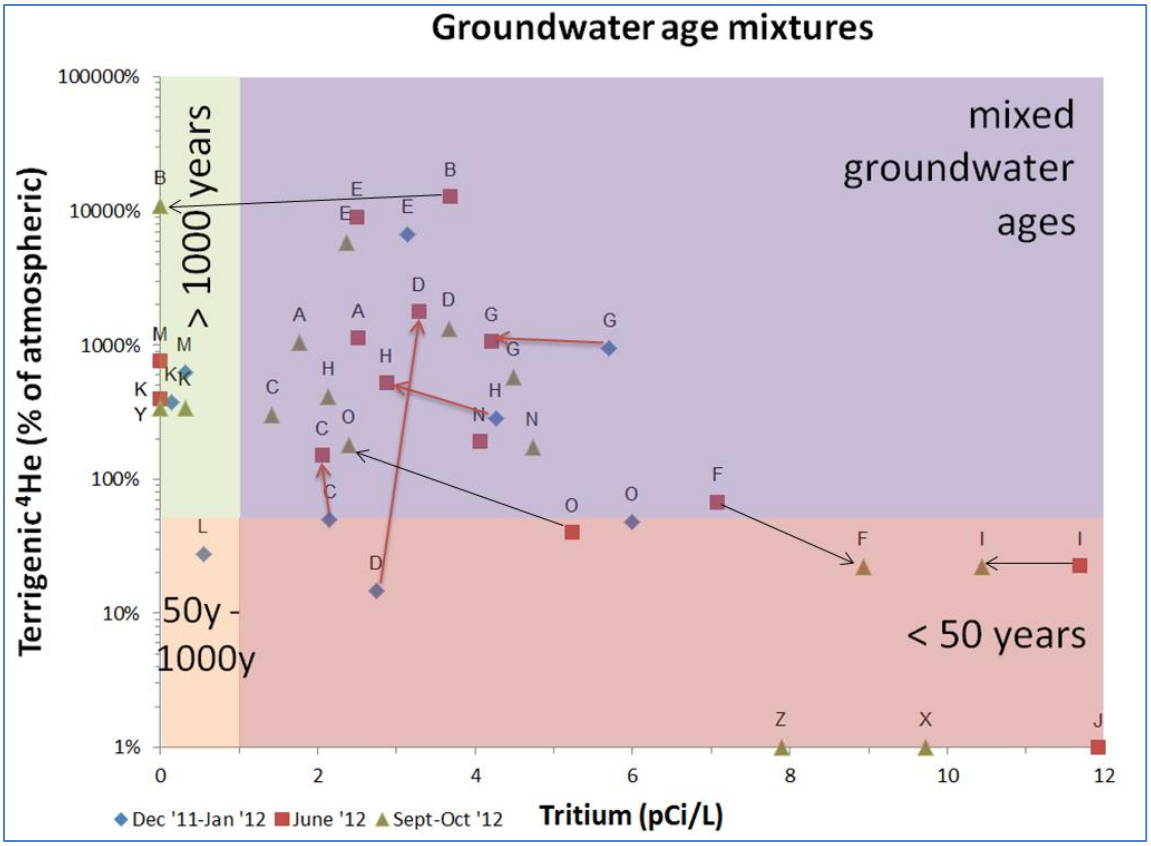

Figure 18: The four groundwater age classifications explained in Table 3 are shown as shaded rectangles. Martis Valley's production wells alternate seasonally drawing more heavily on aquifers with younger (high tritium, low terrigenic ^{4}He) and older (low tritium, high terrigenic ^{4}He) components of groundwater. Red and black arrows point out significant changes in groundwater composition from winter to summer and from summer to fall sampling events, respectively.

Climate Change Vulnerability

Martis Valley groundwater recharge temperatures and excess air concentrations indicate that groundwater recharge in Martis Valley is occurring primarily in the lower

330 m of the watershed. Climate change may have significant impact on this pattern. If climate change shifts the snowmelt hydrograph to an earlier and sharper peak, then groundwater recharge of snowmelt will likely decrease, and runoff to the Truckee River will likely increase, increasing the potential for flooding. A greater proportion of precipitation falling as rain may mitigate some of negative impacts on recharge and mitigate or exacerbate the negative impacts on flooding, depending on the intensity of the rainfall events.

The seasonal variations in tritium and terrigenic helium found in mixed groundwater show that some production wells (particularly wells C, D, F, I, and O) are relying on significant amounts of younger groundwater for portions of their water during certain times of the year. Wells with the shallowest calculated flow depths and the highest tritium concentrations also show the greatest seasonal variability in groundwater source, and are likely to be the first to be affected by climate-driven change in recharge patterns.

The Polaris Fault and Mantle helium

The Martis Valley basin lies between the Sierra Nevada crest to the west and the Carson Range to the east. This region is part of the Walker Lane Belt shear zone. A combination of Basin and Range style normal faulting as well as strike slip faulting associated with the Walker Lane Belt is responsible for the formation of Martis Valley. Faulting began during the late Miocene and continues to present day with most structural development having occurred during the last five million years (California Groundwater

Bulletin 118, 2006). Martis Valley is bounded by a quaternary aged fault to the west and an active fault in the east. This active fault was recently discovered using Light Detection and Ranging (LiDaR) imaging (Hunter et al., 2011). The fault, since named the Polaris Fault, poses a significant seismic hazard for the region especially because of its close proximity to the earthen Martis Creek Dam. A maximum earthquake magnitude between 6.4 and 6.9 has been estimated for the fault using surface rupture lengths and depths to the base of the seismogenic zone (Hunter et al., 2011).

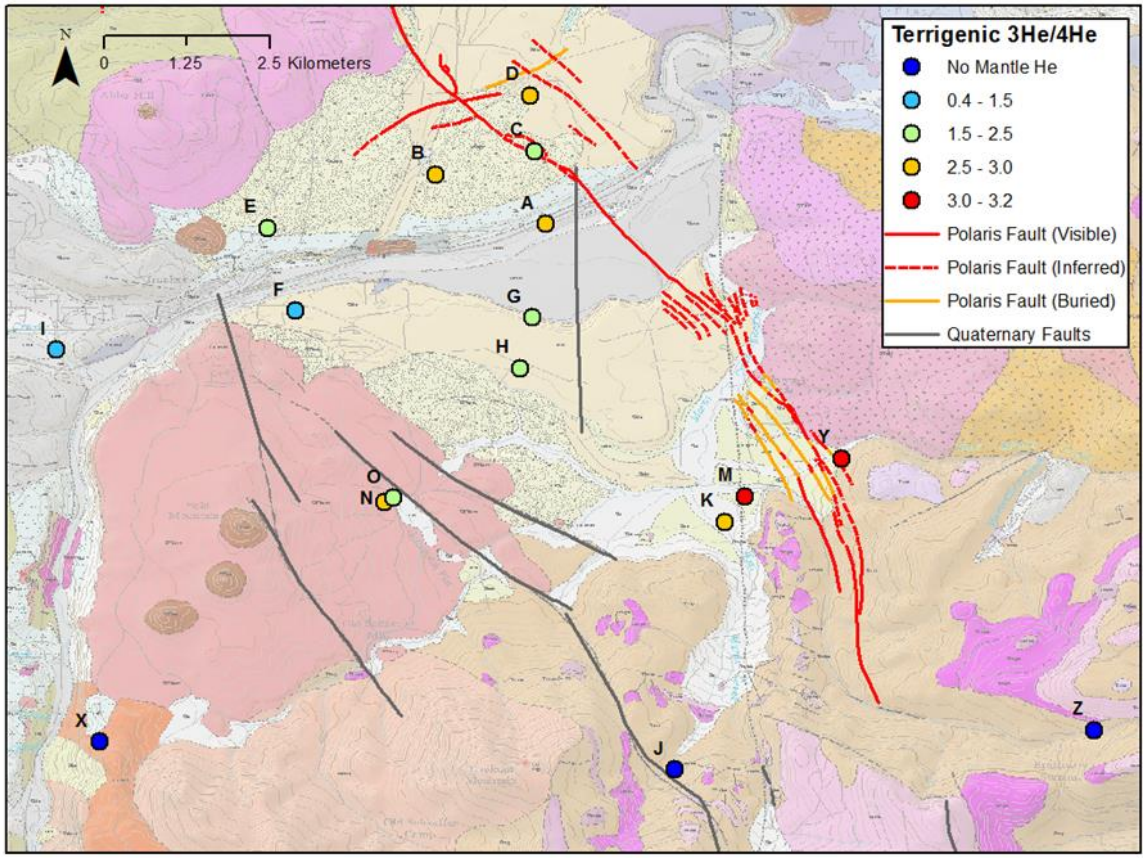

Figure 19: Wells adjacent to the seismically active Polaris fault contain high ratios of terrigenic $^{3}He/^{4}He$ to atmospheric $^{3}He/^{4}He$. (Shown with geological map (Sylvester et al., 2007) and Polaris Fault (Hunter et al., 2011).).

Mantle helium has been found in groundwater in basins where active faulting is occurring along the active San Andreas fault system (Kennedy, 1997). In Martis Valley, a discernible pattern exists in the spatial distribution of wells containing mantle helium (Figure 19). In general, wells adjacent to the seismically active Polaris fault contain relatively high ratios of terrigenic $^{3}He/^{4}He$, indicating the presence of mantle helium and wells farther from the fault have lower ratios. This relationship is plotted in Figure 20 in which a regression line shows a correlation between terrigenic $^{3}He/^{4}He$ and distance from the Polaris Fault. Wells found on the opposite slopes of Martis Valley or those likely up gradient from the Polaris Fault are also shown in Figure 20, but were excluded from the regression analysis. A spring flowing from near the mapped location of the Polaris Fault (Sample Y on Figure 20), and likely related to the fault, has a terrigenic $^{3}He/^{4}He$ composition close to the terrigenic end-member composition (as determined from the relationship of helium isotopic composition to helium concentration, Figure 17). There is also a positive correlation between the average depth of a well screen and its terrigenic $^{3}He/^{4}He$ ratio (Figure 20). Combining these two factors by dividing a well's distance from the Polaris Fault by the average depth of its well screen yields a much stronger correlation – deep wells near the fault have the highest concentrations of mantle helium (Figure 20). This suggests that the Polaris Fault is a significant conduit for the mantle helium found in Martis Valley's wells. The decrease in mantle helium found in wells

with shallower well screen depths is probably due to dilution from younger groundwater, while deeper well screens sample groundwater sources with a less diluted mantle signal. However, the presence of mantle helium was not correlated with groundwater flow depth alone. This supports the hypothesis that the source of mantle helium occurs in discrete locations, such as faults, which act as conduits for mantle fluids. Wells N and O are located on the western slope of Martis Valley opposite the Polaris Fault, yet contain relatively high levels of mantle helium. They are also situated near the quaternary aged fault, which is believed to be inactive, that bounds Martis Valley to the west. The presence of mantle helium suggests that this fault may still be active.

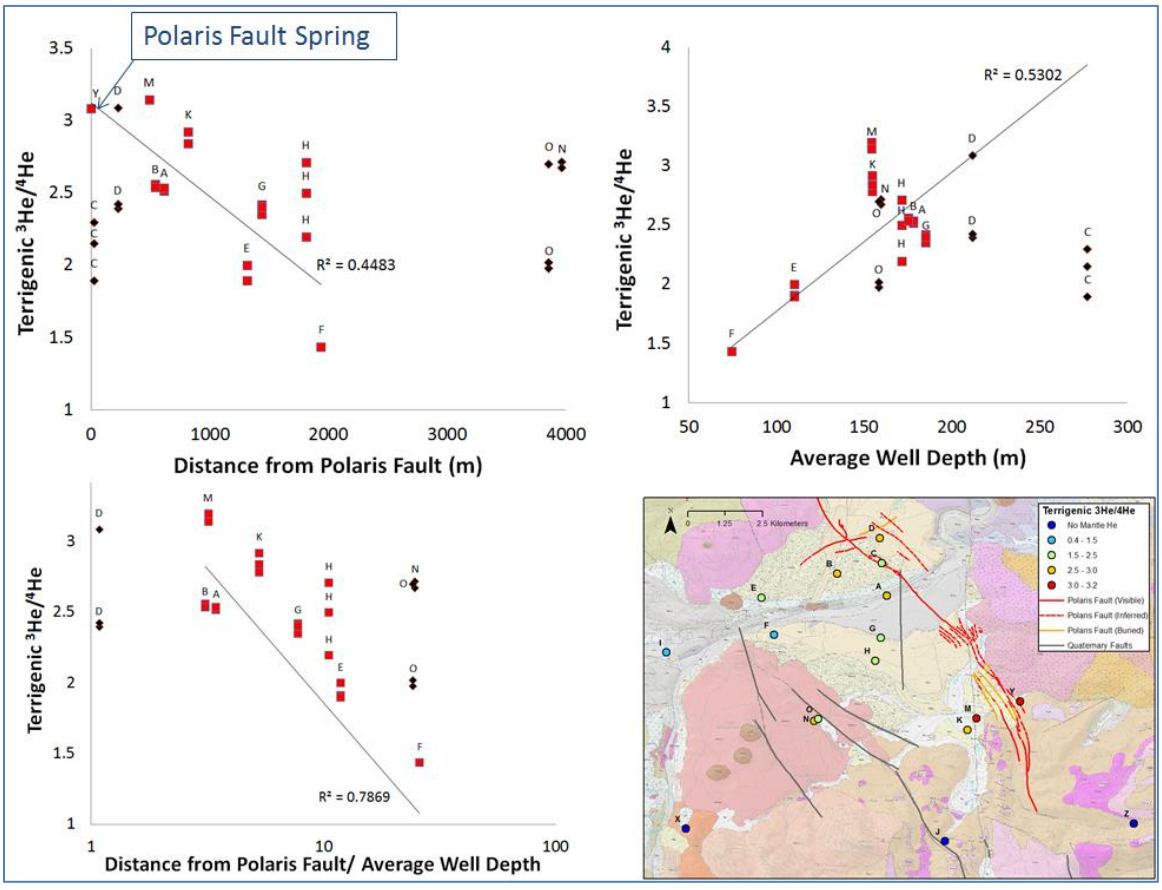

Figure 20: Higher concentrations of mantle helium, represented by higher terrigenic $^{3}He/^{4}He$ ratios, are correlated to the well's distance from the Polaris Fault as well as the well's average screen depth.

The presence of mantle helium, as revealed by a high ratio of terrigenic $^{3}He/^{4}He$ to atmospheric $^{3}He/^{4}He$, can be used as a tracer of groundwater flow in Martis Valley. Spatial interpolation of the terrigenic $^{3}He/^{4}He$ ratios can be used to distinguish two groundwater sources (Figure 21). One source, shown in red, contains groundwater likely to entrain fluids as it passes through the Polaris Fault zone, becoming enriched in mantle helium. The other source, shown in blue, flows from Martis Valley's slopes perpendicular to the trend of the Polaris Fault, mainly from the west. The blue source will contain groundwater with little mantle helium, especially if the Polaris Fault is the main source of mantle helium. Figure 21 reveals areas where mixing between these two sources is likely occurring. In the southeast, the main source of recharge is up gradient from the Polaris Fault. Water picks up mantle helium as it flows through the fault resulting in high levels of mantle helium in wells M, K, and spring Y. Mixing of the two sources is probably responsible for the moderate mantle helium values found in Wells G and H, which are located down gradient and with increasing distance from the fault. Groundwater flowing across the Polaris Fault from the north is responsible for bringing mantle helium to wells A and B. Wells I and F are located up gradient from the Fault so they contain relatively little mantle helium. In general, groundwater flowpaths suggested by the terrigenic $^{3}He/^{4}He$ ratio correspond with the trends inferred from hydraulic head data (Brown&Caldwell, 2013) and roughly follow the topography of Martis Valley. Well

C is located between two inferred segments of the Polaris Fault, but contained lower mantle helium than expected. However, this well was sampled by the USGS in 2007 and was found to contain a higher terrigenic $^{3}He/^{4}He$ ratio of 2.51. A possible explanation for this change in the terrigenic $^{3}He/^{4}He$ ratio over the last 5 years could be a change in the groundwater source being pumped, or a shift in groundwater flow direction.

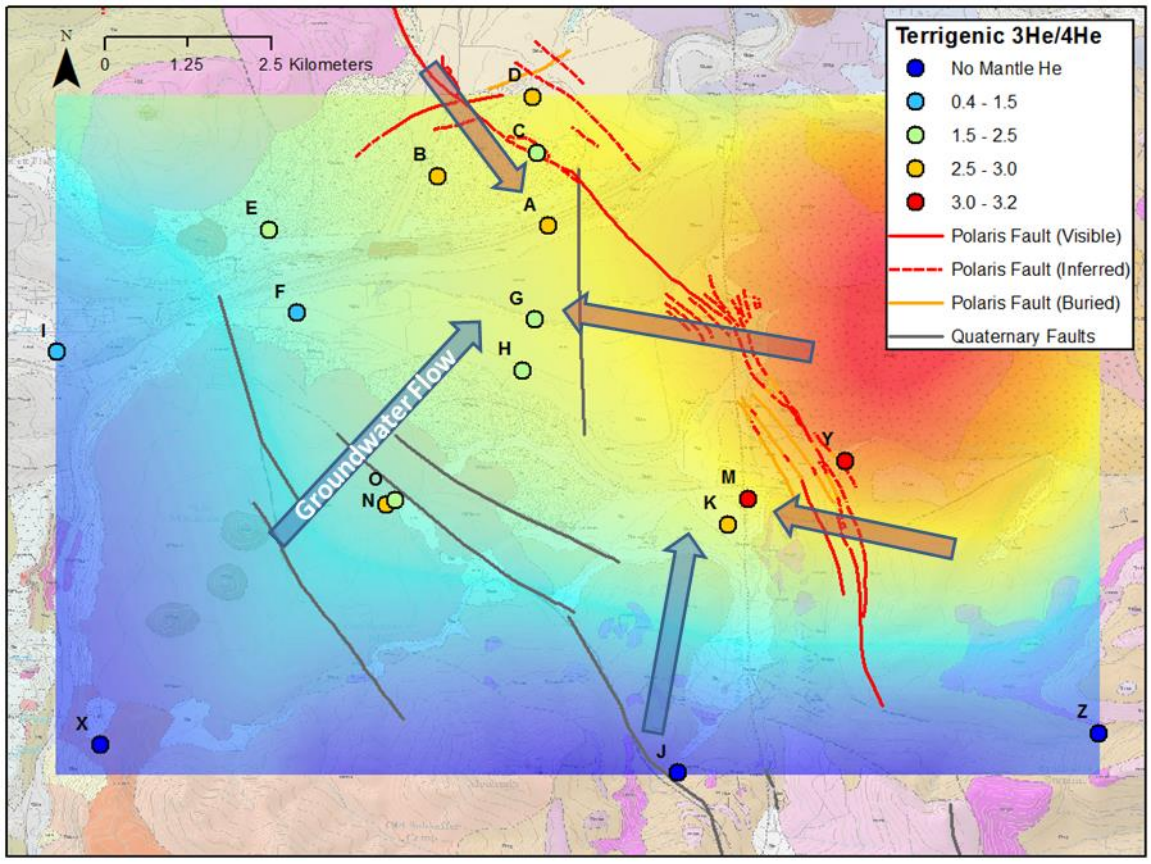

Figure 20: Groundwater in Martis Valley that recharged in areas on the map shown in red may entrain mantle helium during transport toward the valley floor, as this water will likely pass through the zone influenced by the Polaris Fault. Groundwater that recharged in blue areas will contain little mantle helium, especially if the Polaris Fault is the main

source of mantle helium. Red and blue arrows show inferred groundwater flow directions from these two recharge areas (Shown with geological map (Sylvester et al., 2007) and Polaris Fault (Hunter et al., 2011).).

The theory that relatively high concentrations of mantle helium found in the wells originated from the Polaris Fault would require advective flow in the Martis Valley groundwater basin. The time it would take for mantle helium to decrease in concentration solely by diffusion from the Polaris Fault end member composition (terrigenic $^{3}He/^{4}He$ ratio of 3.0) to the concentration measured at each well, located various distances from the fault, was calculated. Wells A and G took 25 million years and 78 million years, respectively, assuming a helium diffusivity of $5.6x10^{-9}$ m^2 s^{-1}. This is much slower than the predicted residence time for groundwater in the basin, confirming that advection is the main driver of groundwater flow and mixing.

Mantle Helium in California

The mechanisms which bring mantle helium into shallow groundwater systems are poorly understood, but improved understanding could potentially lead to a predictive tool by which mantle helium in groundwater indicates potential for seismicity along active faults. Figure 22 shows the ratio of terrigenic $^{3}He/^{4}He$ to atmospheric $^{3}He/^{4}He$ for all the wells in California analyzed by the LLNL noble gas laboratory under the State Water Resources Control Board Groundwater Ambient Monitoring and Assessment (GAMA) program (waterboards.ca.gov/gama/). In Northern California, in addition to wells in proximity to Martis Valley's Polaris Fault, high levels of mantle helium

(terrigenic $^{3}He/^{4}He$: Ra>3) were found in wells located between the San Andreas, Calaveras, and Hayward Faults (Figure 23). In Southern California, high levels of mantle helium were found near the Murrieta Creek Fault and an unnamed fault near Coyote Hill (both active segments of the Elsinore Fault), as well as along the San Andreas Fault near the junction between the Garlock Fault and the San Andreas Fault (Figure 24). Each one of these faults with nearby wells containing high levels of mantle were identified as strike-slip faults active within the last 150 years. Strike-slip faults may provide a conduit for mantle helium to reach groundwater, since they deliver a direct vertical path normal to the mantle, unlike normal or thrust faults, which tend to become more parallel to the crust-mantle boundary at depth. It should be noted that not all wells near active strike-slip faults contained mantle helium, indicating that other geological or hydrogeological conditions must be present in order to create a path for mantle helium to enter into a shallow aquifer.

The Polaris Fault is located in region experiencing extension, while the intersection of the San Andreas Fault and the Garlock Fault is experiencing compression. The Elsinore, Calaveras, and Hayward Faults are parallel to the San Andreas Fault, but are slipping at different rates.

High mantle helium was also found in wells near Mt. Lassen and Mt. Shasta in the Cascade Range. Magma chambers from these volcanoes and associated faulting is likely responsible for bringing mantle helium into overlying groundwater at these locations.

Higher helium concentrations in soil gas have long been reported along the San Andreas Fault. Attempts to use increases in helium concentrations as a tool to predict earthquakes have been controversial and have produced mixed results (Reimer, 1985). In general, $^{3}He/^{4}He$ ratios found in groundwater and drilling fluids tend to increase with proximity to the San Andreas Fault (Kennedy, 1997; Kulongoski et al., 2013; Wiersberg and Erzinger, 2011). Explanations for the spatial variability in $^{3}He/^{4}He$ ratios found near the fault include episodic faulting or fracturing (Nur and Walder, 1990) or variations in fluid flow depth due to differing permeability in the country rock (Wiersberg and Erzinger, 2011). Advective flow also likely plays a role in distributing helium in the shallow crust where it mixes with radiogenic helium thereby lowering the $^{3}He/^{4}He$ ratio (Kulongoski et al., 2013). In the Long Valley caldera, higher $^{3}He/^{4}He$ ratios were found to be correlated with higher levels of seismicity, although the effect of the location, frequency, and magnitude of seismic events are difficult to quantify (Hilton, 1995).

Future studies are needed to determine whether mantle helium can be used to assess seismic risk. The sampling points shown in Figures 21-23 are not ideal for examining spatial variability and how it relates to seismicity since they represent different well depths, screened intervals, and pump rates. Deeper well depth in particular was shown to be associated with higher mantle helium concentrations in Martis Valley.

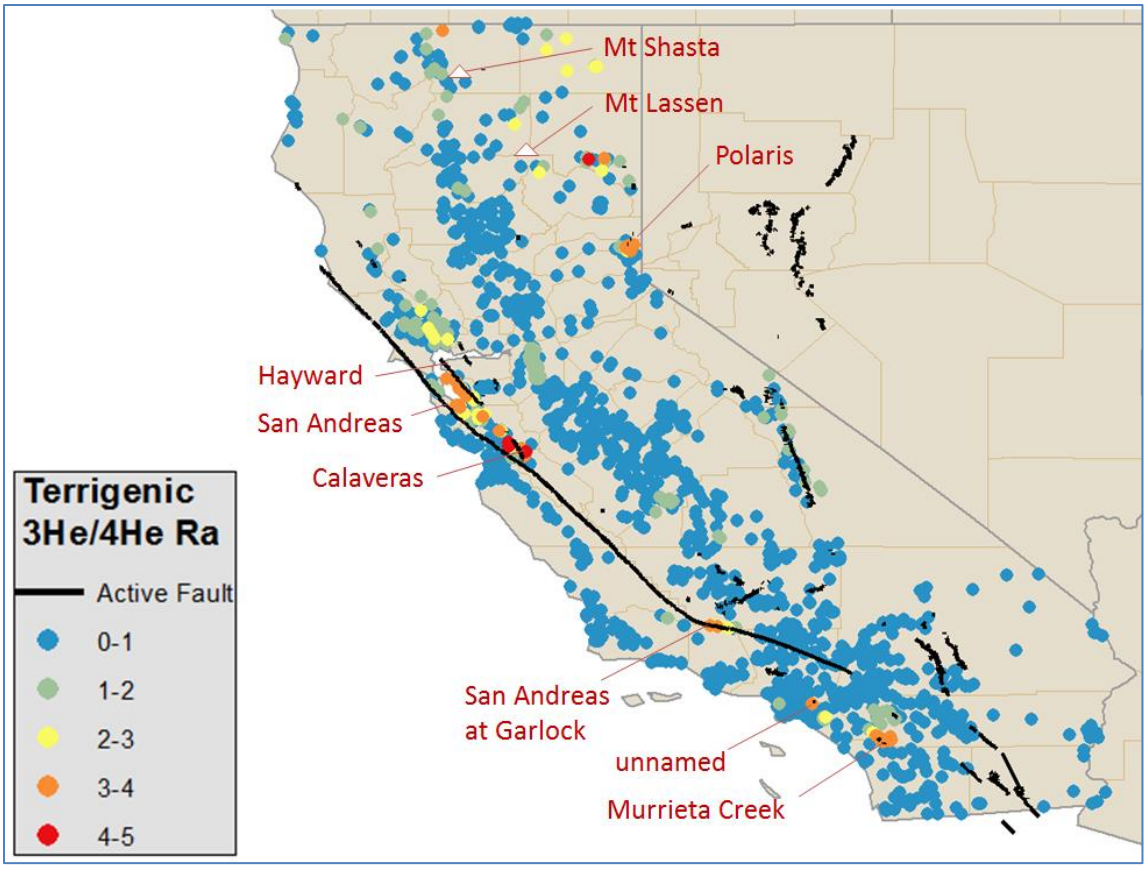

Figure 22: Map of wells in California with measured ratios of terrigenic $^{3}He/^{4}He$ to atmospheric $^{3}He/^{4}He$. High ratios (>3) were found only near a subset of active strike-slip faults.

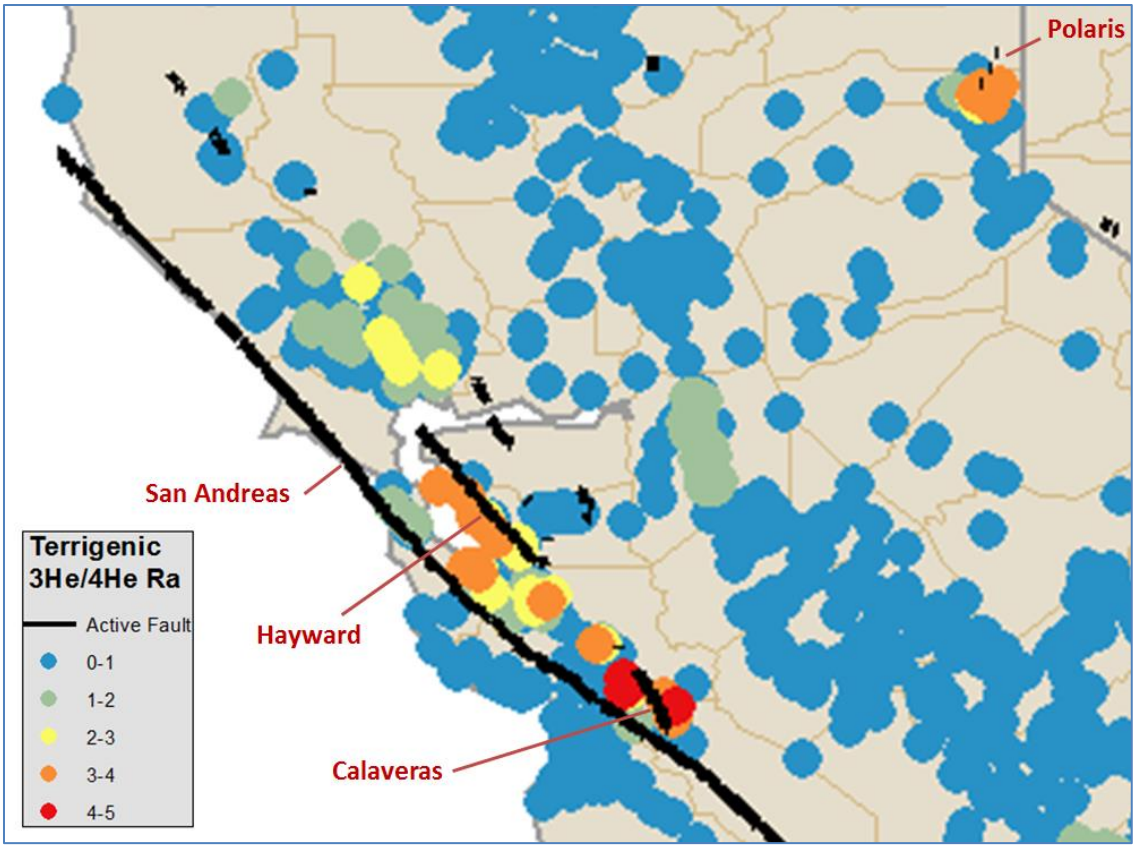

Figure 22: Map of wells in Northern California with measured ratios of terrigenic $^{3}He/^{4}He$ to atmospheric $^{3}He/^{4}He$.

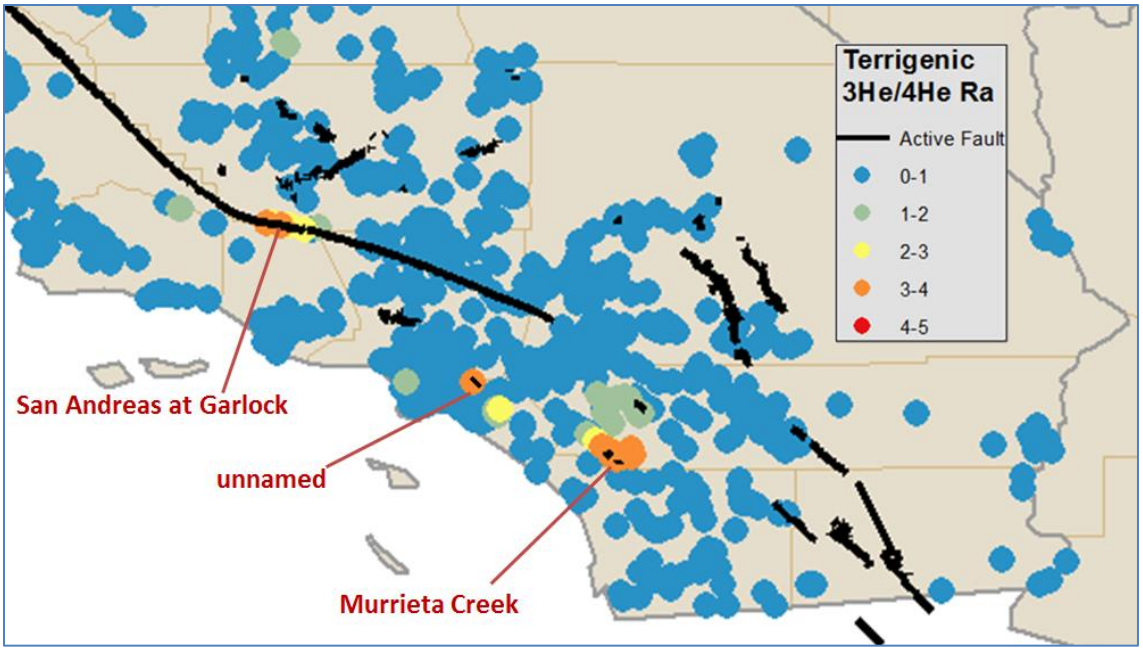

Figure 23: Map of wells in Northern California with measured ratios of terrigenic $^{3}He/^{4}He$ to atmospheric $^{3}He/^{4}He$.

CONCLUSION

Dissolved gases and isotopes provide valuable insights into the groundwater conditions and flow in Martis Valley and are useful in evaluating the potential impact climate change will have on the local groundwater supply. Long screened wells produce groundwater with mixtures of ages, from less than 50 years (containing tritium) to over 1000 years (containing terrigenic helium). Seasonal variations in recharge temperatures, tritium, and excess air suggest that the wells capture water masses of varying recharge conditions and groundwater ages throughout the year. Wells with shallow flow depths show significant seasonal variability, making them particularly vulnerable to effects from climate change. Mantle helium originating from the Polaris Fault can be used to trace groundwater flow directions and mixing of different groundwater sources. Wells in California found to contain high levels of mantle helium are exclusively located in volcanically active regions or adjacent to active strike-slip faults. More studies are needed to understand the mechanisms that bring mantle helium into shallow groundwater systems in order to determine if mantle helium can be used to measure seismic risk. Dissolve gases and isotopes can be valuable tools for aquifer characterization. The interpretation of groundwater conditions in Martis Valley based on measurements of dissolved gases and isotopes could not have been determined from conventional hydrogeological methods.

REFERENCES

Aeschbach-Hertig, W., El-Gamal, H., Wieser, M., and Palcsu, L., 2008, Modeling excess air and degassing in groundwater by equilibrium partitioning with a gas phase: Water Resources Research, v. 44, no. 8, p. n/a-n/a.

Ajami, H., Troch, P. A., Maddock, T., Meixner, T., and Eastoe, C., 2011, Quantifying mountain block recharge by means of catchment-scale storage-discharge relationships: Water Resources Research, v. 47, no. 4, p. n/a-n/a.

Benson, B., 1973, Noble gas concentration ratios as paleotemperature indicators: Geochimica et cosmochimica acta, v. 37, no. 5, p. 1391-1395.

Beyerle, U. R. S., and Du, C.-. 2000, A Mass Spectrometric System for the Analysis of Noble Gases and Tritium from Water Samples, v. 34, p. 2042-2050.

Brown&Caldwell, 2013, Martis Valley Groundwater Management Plan.

California Groundwater Bulletin 118, 2006, Martis Valley Groundwater Basin.

Cey, B. D., Hudson, G. B., Moran, J. E., and Scanlon, B. R., 2009, Evaluation of noble gas recharge temperatures in a shallow unconfined aquifer: Ground Water, v. 47, no. 5, p. 646-659.

Coulter, T., DeVore, C., Hall, R., Johnson, M., Kinkel, B., Klumpp, C., Larsen, D., Leffel, S., Levitsky, S., Parr, K., Scott, T., Strekal, T., and Whitfield, J., 2009, Truckee River Operating Agreement Final EIS/EIR.

Craig, H., Lupton, J. E., Welhan, J.A., Poreda, R., 1978, Helium isotope ratios in Yellowstone and Lassen Park volcanic gases: Geophysical Research Letters, v. 5, no. 11, p. 897-900.

Earman, S., and Dettinger, M., Long-term Recharge Change in the Mountains of California and Nevada2007.

Flint, A. L., Flint, L. E., and Dettinger, M. D., 2008, Modeling Soil Moisture Processes and Recharge under a Melting Snowpack: Vadose Zone Journal, v. 7, no. 1, p. 350.

Fram, M., Munday, C., and Belitz, K., Groundwater Quality Data for the Tahoe – Martis Study Unit , 2007 : Results from the California GAMA Program 2009.

Heaton, T. H. E., and Vogel, J. C., 1981, "Excess air" in groundwater: Journal of Hydrology, v. 50, p. 201-216.

Hilton, D. R., 1995, The helium and carbon isotope systematics of a continental geothermal system: results from monitoring studies at Long Valley caldera (California, U.S.A.): Chemical Geology, no. 127, p. 269-295.

Hudson, G. B., and Moran, J. E., 2002, Delineation of Fast Flow Paths in Porous Media Using Noble Gas Tracers: Lawrence Livermore National Laboratory UCRL-ID-147734.

Hunter, L. E., Howle, J. F., Rose, R. S., and Bawden, G. W., 2011, LiDAR-Assisted Identification of an Active Fault near Truckee, California: Bulletin of the Seismological Society of America, v. 101, no. 3, p. 1162-1181.

Huntington, J. L., Niswonger, R. G., Rajagopal, S., Gardner, Y. Z. M., Morton, C. G., Reeves, D. M., McGraw, D., and Pohll, G. M., 2013, Integrated Hydrologic Modeling of Lake Tahoe and Martis Valley Mountain Block and Alluvial Systems, Nevada and California.

James, E. R., Manga, M., Rose, T. P., and Hudson, G. B., 2000, The use of temperature and the isotopes of O, H, C, and noble gases to determine the pattern and spatial extent of groundwater flow: Journal of Hydrology, v. 237, no. 1-2, p. 100-112.

Kennedy, B. M., 1997, Mantle Fluids in the San Andreas Fault System, California: Science, v. 278, no. 5341, p. 1278-1281.

Klump, S., Tomonaga, Y., Kienzler, P., Kinzelbach, W., Baumann, T., Imboden, D. M., and Kipfer, R., 2007, Field experiments yield new insights into gas exchange and excess air formation in natural porous media: Geochimica et Cosmochimica Acta, v. 71, no. 6, p. 1385-1397.

Kulongoski, J. T., Hilton, D. R., Barry, P. H., Esser, B. K., Hillegonds, D., and Belitz, K., 2013, Volatile fluxes through the Big Bend section of the San Andreas Fault, California: Helium and carbon-dioxide systematics: Chemical Geology, v. 339, p. 92-102.

Manning, A. H., and Caine, J. S., 2007, Groundwater noble gas, age, and temperature signatures in an Alpine watershed: Valuable tools in conceptual model development: Water Resources Research, v. 43, no. 4, p. 16.

Mazor, E., 1972, Paleotemperatures and Other Hydrological Parameters Deduced from Noble-Gases Dissolved in Groundwaters - Jordan Rift Valley, Israel: Geochimica et Cosmochimica Acta, v. 36, no. 12, p. 1321-&.

Michel, R. L., and Schroeder, R. A., 1994, Use of long-term tritium records from the Colorado River to determine timescales for hydrologic processes associated with

irrigation in the Imperial Valley, California: Applied Geochemistry, v. 9(4), p. 387-401.

Moran, J. E., McNab, W. W., Esser, B. E., and Hudson, G. B., 2005, California GAMA program: Sources and transport of nitrate in shallow groundwater in the Llagas Basin of Santa Clara County, California: Lawrence Livermore National Laboratory, UCRL-TR-213705.

Nimbus Engineers, 2001, Ground Water Availability in the Martis Valley Ground Water Basin.

Nur, A., and Walder, J., 1990, Time-dependent hydraulics of the Earth's crust. The Role of Fluids in Crustal Processes: National Academy Press, p. 113-127.

Peeters, F., Beyerle, U., and Kipfer, R., 2000, Manual for the program " NOBLE90 ", p. 1-10.

Reimer, G. M., 1985, Prediction of Central California Earthquakes from Soil-Gas Helium Fluctuations: Pageoph, v. 122, p. 369-375.

Saar, M. O., Castro, M. C., Hall, C. M., Manga, M., and Rose, T. P., 2005, Quantifying magmatic, crustal, and atmospheric helium contributions to volcanic aquifers using all stable noble gases: Implications for magmatism and groundwater flow: Geochemistry, Geophysics, Geosystems, v. 6, no. 3, p. n/a-n/a.

Singleton, M., and Hudson, B., 2005, Membrane Inlet Mass Spectrometry for measuring dissolved gases: Lawrence Livermore National Laboratory.

Singleton, M. J., and Moran, J. E., 2010, Dissolved noble gas and isotopic tracers reveal vulnerability of groundwater in a small, high-elevation catchment to predicted climate changes: Water Resources Research, v. 46, no. 12, p. n/a-n/a.

Stute, M., Forster, M., Frischkorn, H., Serejo, a., Clark, J. F., Schlosser, P., Broecker, W. S., and Bonani, G., 1995, Cooling of Tropical Brazil (5{degrees}C) During the Last Glacial Maximum.: Science (New York, N.Y.), v. 269, p. 379-383.

Sylvester, A., Wise, W., Hastings, J., and Moyer, L., 2007, New digital geologic map of the northern Lake Tahoe-Donner Pass Region, Sierra Nevada, California, GSA Abstr. Programs, p. 39, no.35.

Torgersen, T., 1980, Controls on pore-fluid concentration of He-4 and Rn-222 and the calculation of He-4-Rn-222 ages: Journal of Geochemical Exploration, v. 13, p. 57.

Visser, A., 2011, Noble gas isotope hydrology: How old is our drinking water?, LLNL Postdoc Seminar (11/15/2011, Livermore, CA). LLNL-PRES-514091.

Wiersberg, T., and Erzinger, J., 2011, Chemical and isotope compositions of drilling mud gas from the San Andreas Fault Observatory at Depth (SAFOD) boreholes: Implications on gas migration and the permeability structure of the San Andreas Fault: Chemical Geology, v. 284, no. 1-2, p. 148-159.